

NASA TECHNICAL NOTE



NASA TN D-3434

C.1

NASA TN D-3434

LOAN COPY: RETURN TO  
AFWL (WLIL-2)  
KIRTLAND AFB, NM

0130159



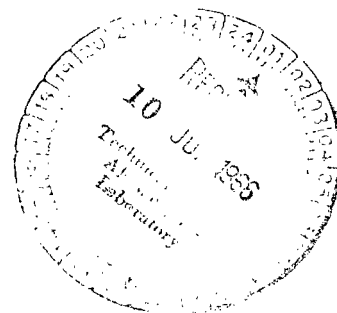
TECH LIBRARY KAFB, NM

CHARTS OF ADDITIVE DRAG COEFFICIENT  
AND MASS-FLOW RATIO FOR INLETS  
UTILIZING RIGHT CIRCULAR CONES  
AT ZERO ANGLE OF ATTACK

by *Vincent R. Mascitti*

*Langley Research Center*

*Langley Station, Hampton, Va.*





0130159

MADE IN U.S.A.

CHARTS OF ADDITIVE DRAG COEFFICIENT AND MASS-FLOW  
RATIO FOR INLETS UTILIZING RIGHT CIRCULAR  
CONES AT ZERO ANGLE OF ATTACK

By Vincent R. Mascitti

Langley Research Center  
Langley Station, Hampton, Va.

NATIONAL AERONAUTICS AND SPACE ADMINISTRATION

---

For sale by the Clearinghouse for Federal Scientific and Technical Information  
Springfield, Virginia 22151 - Price \$2.00

CHARTS OF ADDITIVE DRAG COEFFICIENT AND MASS-FLOW  
RATIO FOR INLETS UTILIZING RIGHT CIRCULAR  
CONES AT ZERO ANGLE OF ATTACK

By Vincent R. Mascitti  
Langley Research Center

SUMMARY

Working charts are presented giving values of additive drag coefficient and mass-flow ratio for inlets utilizing axisymmetric cones at zero angle of attack. Cone half-angles range from  $5^{\circ}$  to  $35^{\circ}$ . The free-stream Mach number ranges from that which will yield sonic flow on the cone surface to 12. Perfect-gas relations are used throughout the calculations.

INTRODUCTION

The treatment of additive drag in reference 1 includes a study of axisymmetric inlets for a limited range of free-stream Mach numbers and cone half-angles which were of primary interest at the time the study was made. Utilizing axisymmetric inlets for hypersonic vehicles requires data over a larger range of Mach numbers and at smaller cone half-angles. Calculations for such data have been made and are presented herein as working charts for a range of Mach numbers from that which will yield sonic flow on the cone surface to 12, and for cone half-angles from  $5^{\circ}$  to  $35^{\circ}$ .

The computation of additive drag was accomplished by numerical integration of the pressures existing along the entering stream tube. The mass-flow ratios were determined from the radial coordinates of the streamline which corresponded to the limits of the pressure integration. The computations of the additive drag and the mass-flow ratio were made by adding a subroutine to a machine computer program which was used to calculate conical flow parameters. The computations of the present paper cover the ranges of variables presented in reference 1 in order that a complete set of data may be obtained from one source. It may be noted from a comparison of the two sets of results that some differences in shock angles exist. The shock angles computed herein agree with those presented in reference 2.

## SYMBOLS AND NOTATIONS

|           |   |
|-----------|---|
| A         | cross-sectional area  |
| $C_{D,a}$ | additive drag coefficient, $\frac{D_a}{qA}$   |
| $D_a$     | additive drag   |
| K         | defined parameter, $\frac{(1 - W_1^2)^{\frac{1}{\gamma-1}} W_{N,1}}{\sin \theta_1}$           |
| L         | integration index for cowl location   |
| M         | Mach number   |
| w         | mass flow   |
| $w/w_0$   | ratio of mass flow entering inlet to that passing through area A under free-stream conditions |
| p         | pressure  |
| q         | dynamic pressure, $\frac{\gamma}{2} p_0 M_0^2$  |
| r         | radius  |
| S         | conical area generated by revolution of a ray   |
| t         | temperature   |
| V         | velocity of flow  |
| $V_{lim}$ | limiting velocity obtained by expanding flow to zero temperature                              |
| W         | ratio of local velocity to limiting velocity, $\frac{V}{V_{lim}}$                             |
| z         | distance along generatrix ray   |
| $\gamma$  | ratio of specific heats, 1.400 for air  |

$\eta$  cone half-angle

$\theta$  ray angle

$\rho$  density

Subscripts:

0 conditions upstream of conical shock

1 conditions just downstream of conical shock

c conditions on cone surface

J numerical integration index

l conditions at cowl location

N conditions normal to shock or ray

t stagnation conditions

### METHOD OF SOLUTION

The solution of the flow field around cones at zero angle of attack has been published in references 3 and 4 and, therefore, will not be repeated herein. In the present investigation, the solution of the conical flow problem was derived by the use of an existing computer program in a manner similar to that of reference 3. Outputs were normal and resultant velocity ratio ( $W_N/W$ ) for a given ray angle, cone half-angle, and free-stream Mach number ( $\theta, \eta, M_0$ ). The values of free-stream Mach number for sonic flow on the cone surface were taken from table 1 of reference 5.

For conical flow, the transition across the shock wave is governed by the oblique shock relations and followed by a continuous isentropic compression to surface conditions. Figure 1 shows a diagram of the flow field and additive drag parameters. The conditions just downstream of the shock and the coordinates of a point on the entering streamline must be defined in order to determine the mass-flow ratio.

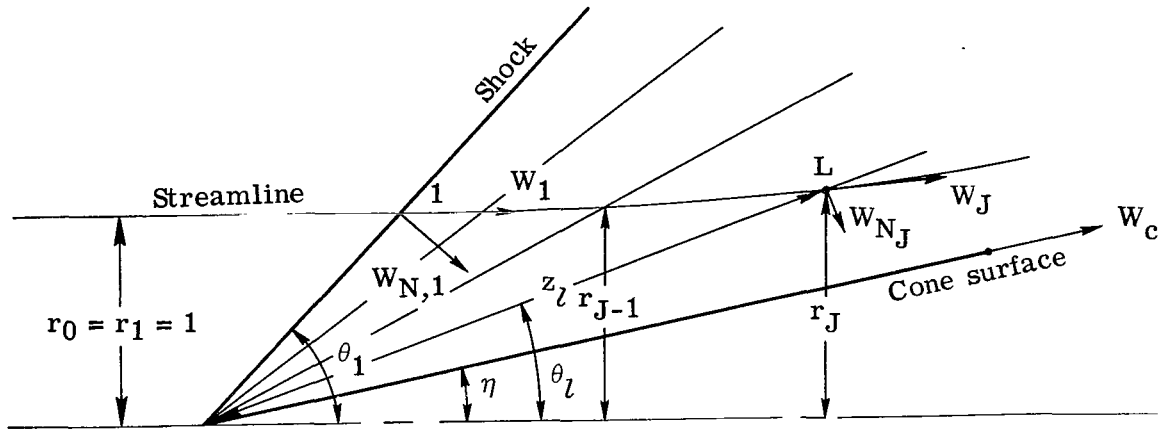


Figure 1.- Diagram showing flow field and additive drag parameters.

The mass flow at any position downstream of the shock is given by

$$w = \rho_l W_{N,l} S_l = \rho_1 W_{N,1} S_1$$

If the following relations are assumed:

$$S_l = \pi r_l z_l$$

$$r_l = z_l \sin \theta$$

$$r_1 = 1$$

$$\left(\frac{\rho}{\rho_t}\right)_l = \left(1 - W_l^2\right)^{\frac{1}{\gamma-1}}$$

the distance along a generatrix ray required to pass the mass flow  $\rho_1 W_{N,1} S_1$  is

$$z_l = \sqrt{\frac{K}{\left(1 - W_l^2\right)^{\frac{1}{\gamma-1}} W_{N,l} \sin \theta_l}}$$

where  $K = \frac{1}{\sin \theta_1} \frac{(1 - W_1^2)^{\gamma-1}}{W_{N,1}}$ , a convenient parameter defined only by conditions across the shock. The mass-flow ratio captured by a cowl lip at position  $l$  is defined as follows:

$$\frac{w}{w_0} = \frac{\rho_0 V_0 A_0}{\rho_0 V_0 A_l}$$

If  $A_l = \pi r_l^2$  and  $r_1 = r_0 = 1$ , then

$$\frac{w}{w_0} = \frac{1}{r_l^2} \quad (1)$$

Additive drag is defined in reference 1 as

$$D_a = \int_1^L (p - p_0) dA \quad (2)$$

Equation (2) may be approximated by the method of numerical integration in the form:

$$D_a = \sum_{J=2}^L \left( \frac{p_J + p_{J-1}}{2} - p_0 \right) (A_J - A_{J-1}) \quad (3)$$

The additive drag coefficient is given by

$$C_{D,a} = \frac{D_a}{qA_l}$$

Substituting equivalent expressions for the parameters in this equation and rearranging yield

$$C_{D,a} = \frac{1}{\gamma M_0^2 r_l^2} \sum_{J=2}^L \left( \frac{p_J}{p_0} + \frac{p_{J-1}}{p_0} - 2 \right) (r_J^2 - r_{J-1}^2)$$

where

$$\frac{p_J}{p_0} = \left( \frac{p_1}{p_0} \right) \left[ \frac{(p/p_t)_J}{(p/p_t)_1} \right]$$

and, from reference 2,

$$\frac{p_1}{p_0} = \frac{2\gamma M_0^2 \sin^2 \theta_1 - (\gamma - 1)}{\gamma + 1}$$

$$\left(\frac{p}{p_t}\right)_J = \left(1 - W_J^2\right)^{\frac{\gamma}{\gamma-1}}$$

The drag coefficient on the cone surface is given by

$$C_{D,c} = \frac{2}{\gamma M_0^2} \left(\frac{p_c}{p_0} - 1\right)$$

where

$$\frac{p_c}{p_0} = \frac{p_1/p_0}{(p/p_t)_1} \left(1 - W_c^2\right)^{\frac{\gamma}{\gamma-1}}$$

Values of the cone drag coefficient are presented in the charts for which  $\theta_l = \eta$ .

In order to obtain sufficient accuracy, a  $0.1^\circ$  ray angle increment for numerical integration was chosen. Increments smaller than  $0.1^\circ$  showed no significant improvement in accuracy.

Perfect-gas relations ( $\gamma = 1.4$ ) are assumed for the calculations herein, but at the higher Mach numbers and cone half-angles this assumption is not correct. The curve in figure 2 indicates the limitations imposed by the assumption. This figure shows the relationship between the cone half-angle and Mach number for which the surface static temperature is  $1000^\circ \text{ R}$  ( $556^\circ \text{ K}$ ). At this temperature the value of  $\gamma$  is 98 percent of the ideal value. At  $M = 12$ , for example, the cone half-angle can be  $11.5^\circ$  without exceeding this temperature limitation. Since at hypersonic speeds the conical half-angles of interest are usually

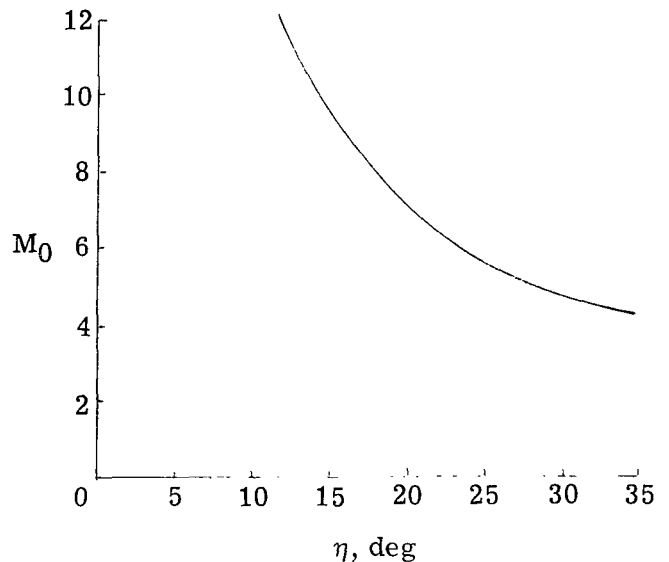
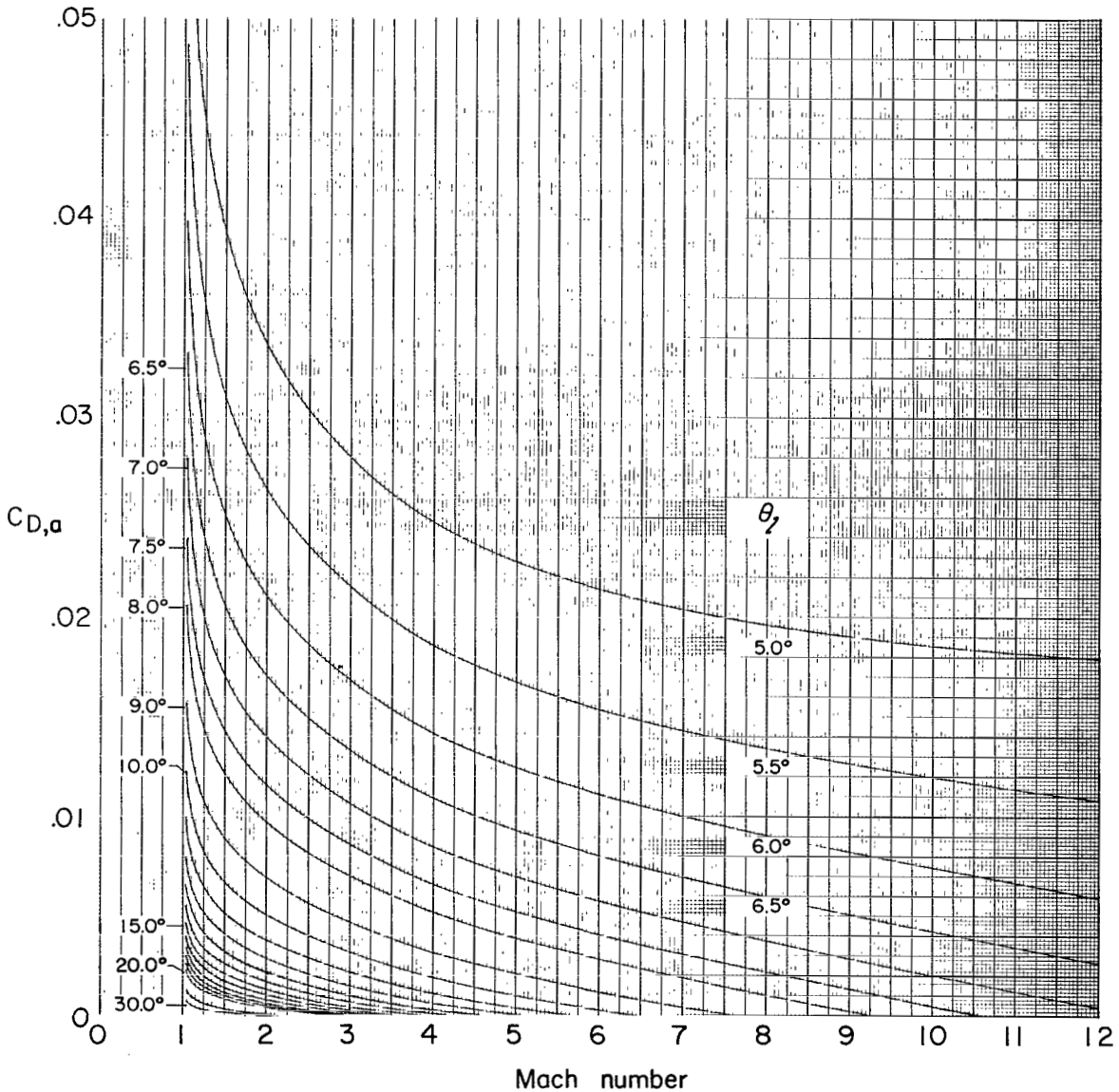


Figure 2.- Variation of free-stream Mach number with cone half-angle for  $t_c = 1000^\circ \text{ R}$  ( $556^\circ \text{ K}$ ).

less than  $10^0$ , expansion of the computation to include effects of the specific-heat ratio was not considered necessary.

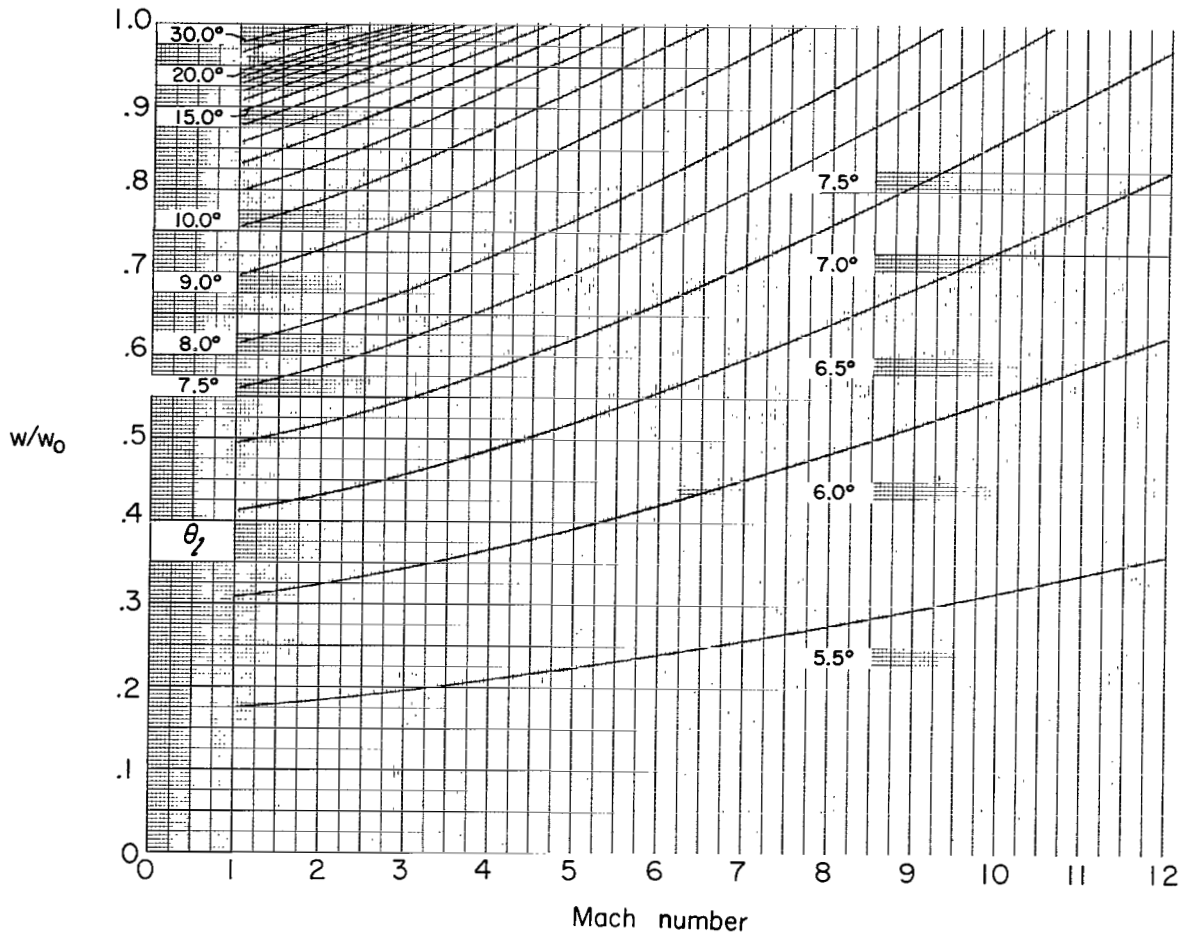
### PRESENTATION OF CHARTS

Working charts are presented for cone half-angles between  $5^0$  and  $35^0$  in figures 3 to 14. For each cone half-angle, the additive drag coefficient is plotted as a function of the free-stream Mach number and the ray angle; the mass-flow ratio is plotted as a function of the free-stream Mach number and the ray angle; and the additive drag coefficient is plotted as a function of the mass-flow ratio for selected free-stream Mach numbers.



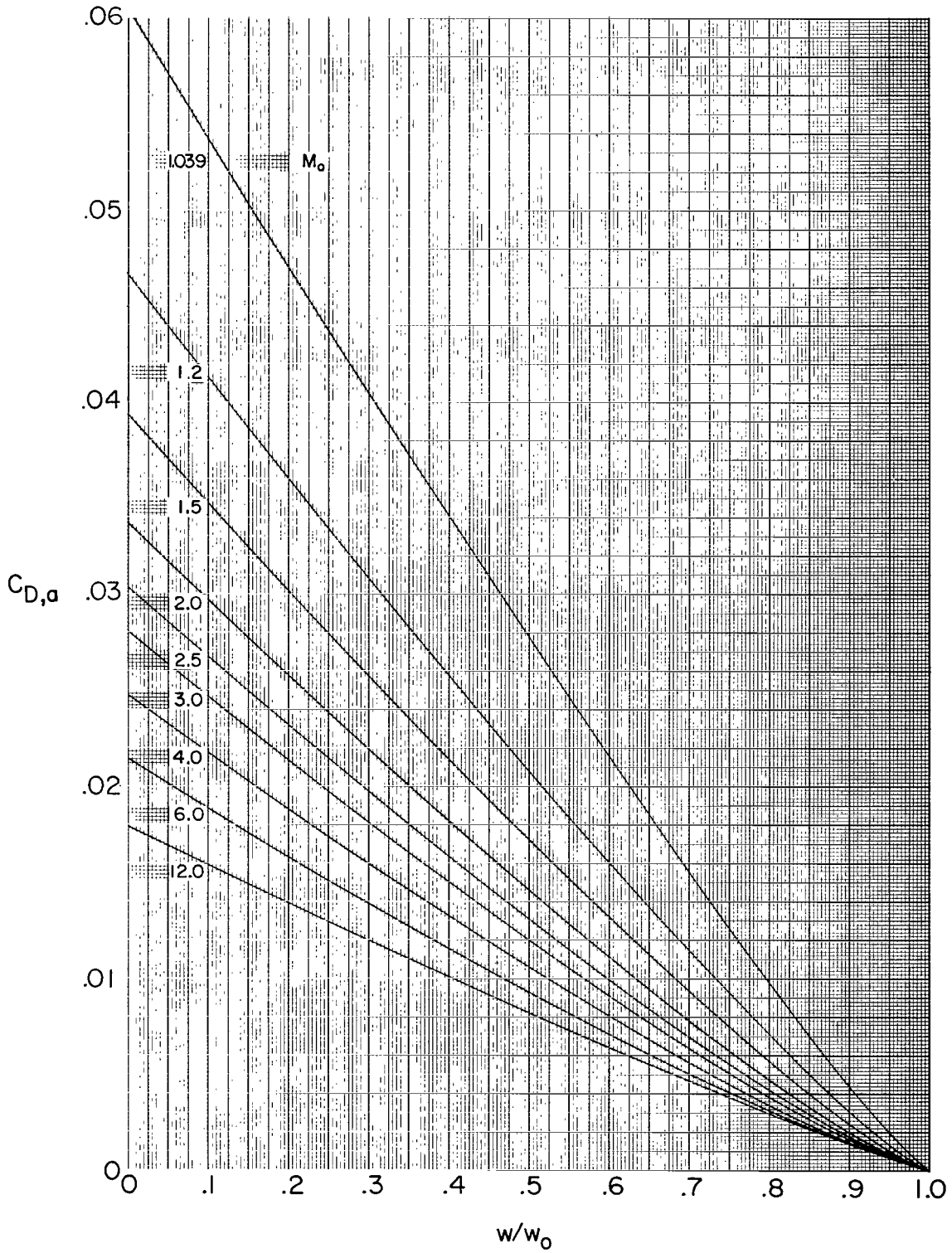
(a) Variation of additive drag with Mach number.

Figure 3.- Variation of additive drag and mass-flow ratio for  $\eta = 5^0$ .



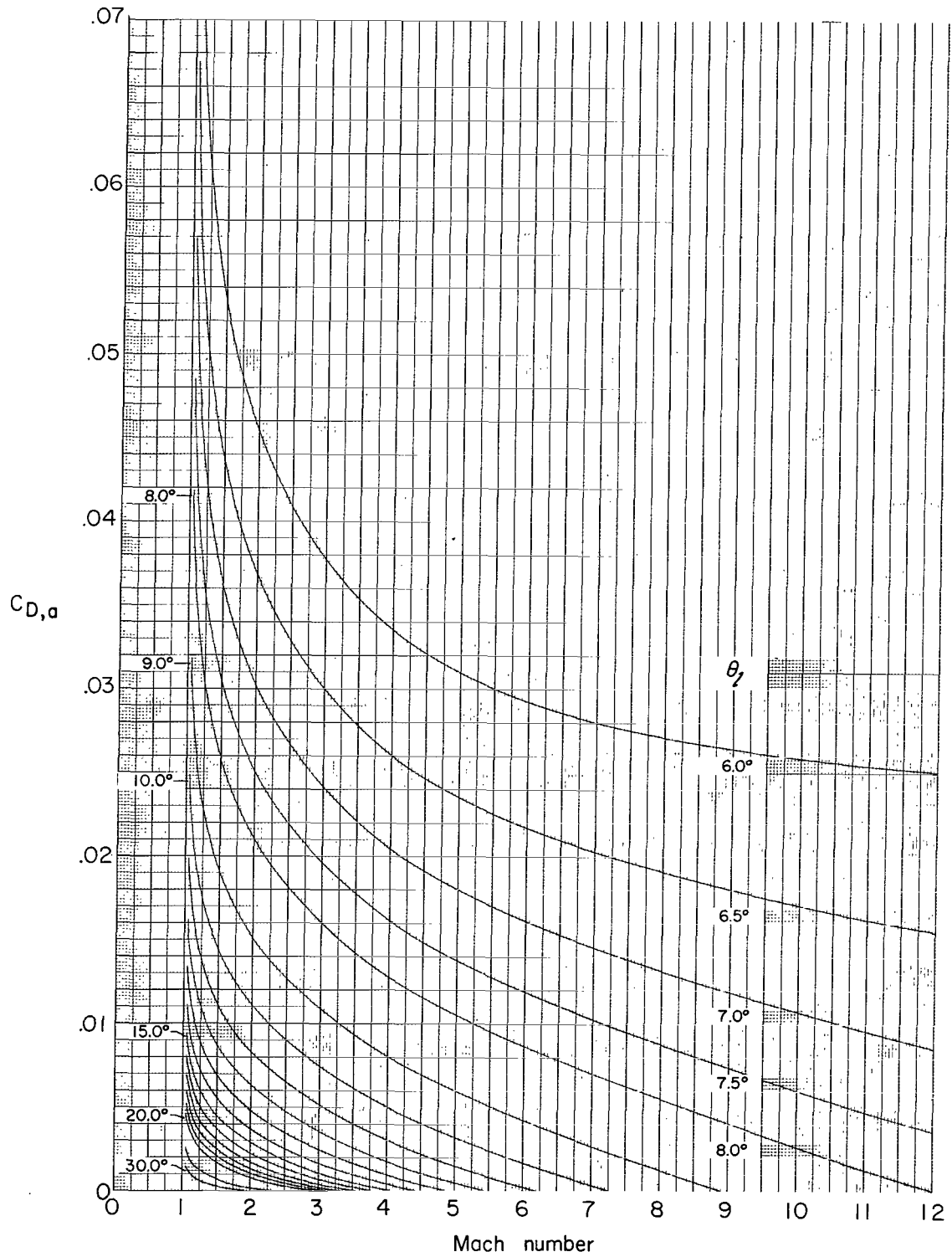
(b) Variation of mass-flow ratio with Mach number.

Figure 3.- Continued.



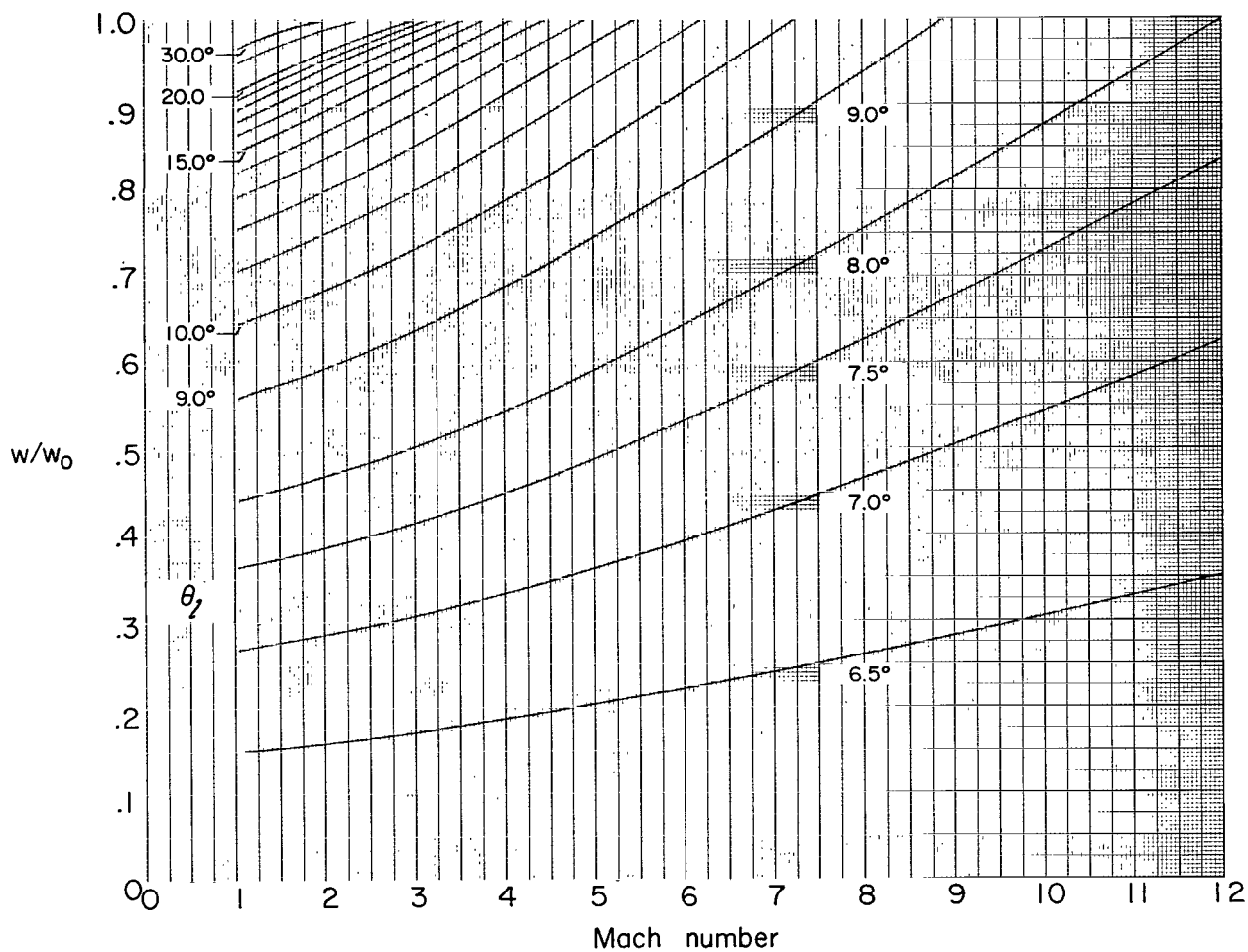
(c) Variation of additive drag with mass-flow ratio.

Figure 3.- Concluded.



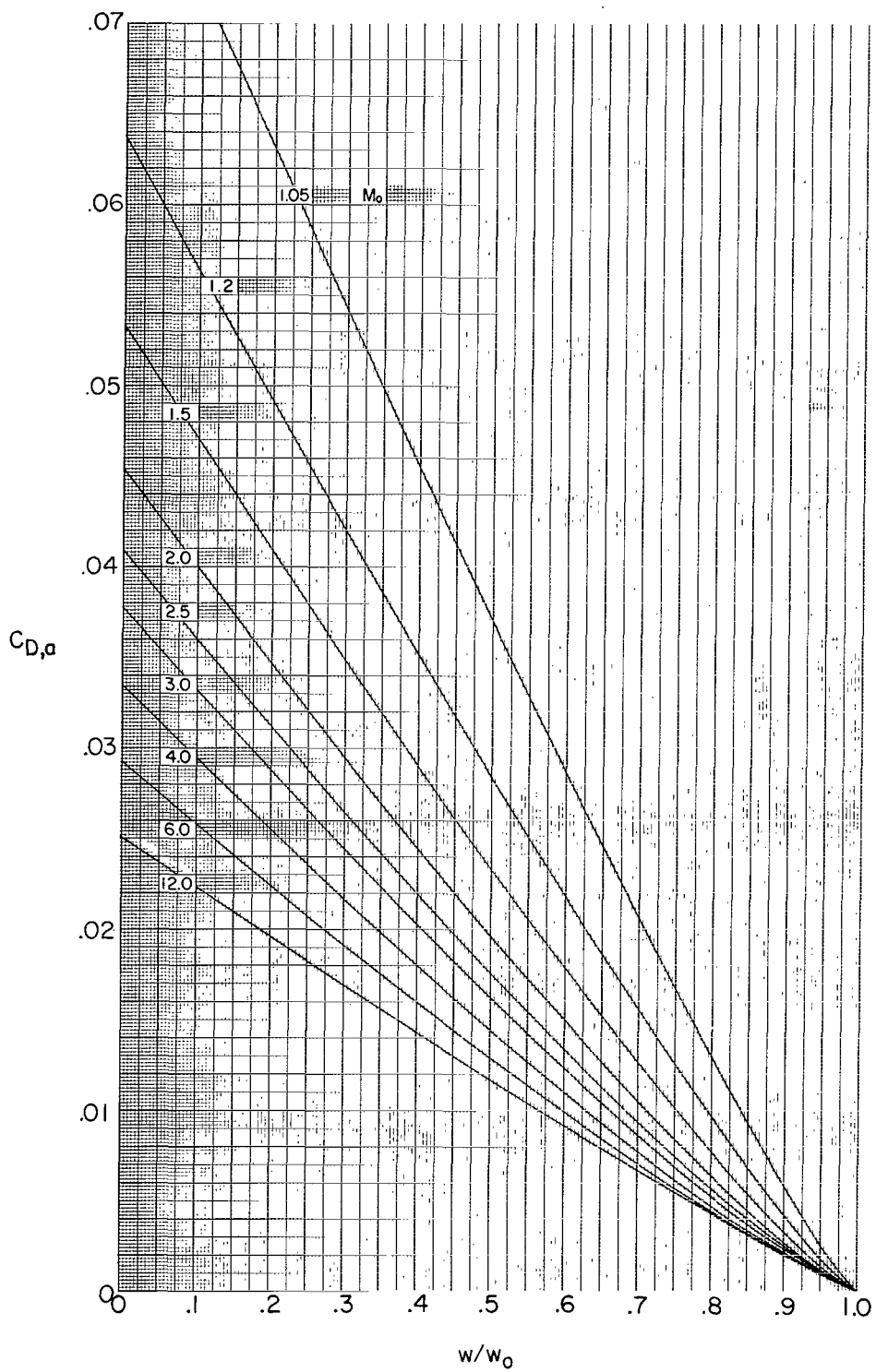
(a) Variation of additive drag with Mach number.

Figure 4.- Variation of additive drag and mass-flow ratio for  $\eta = 60$ .



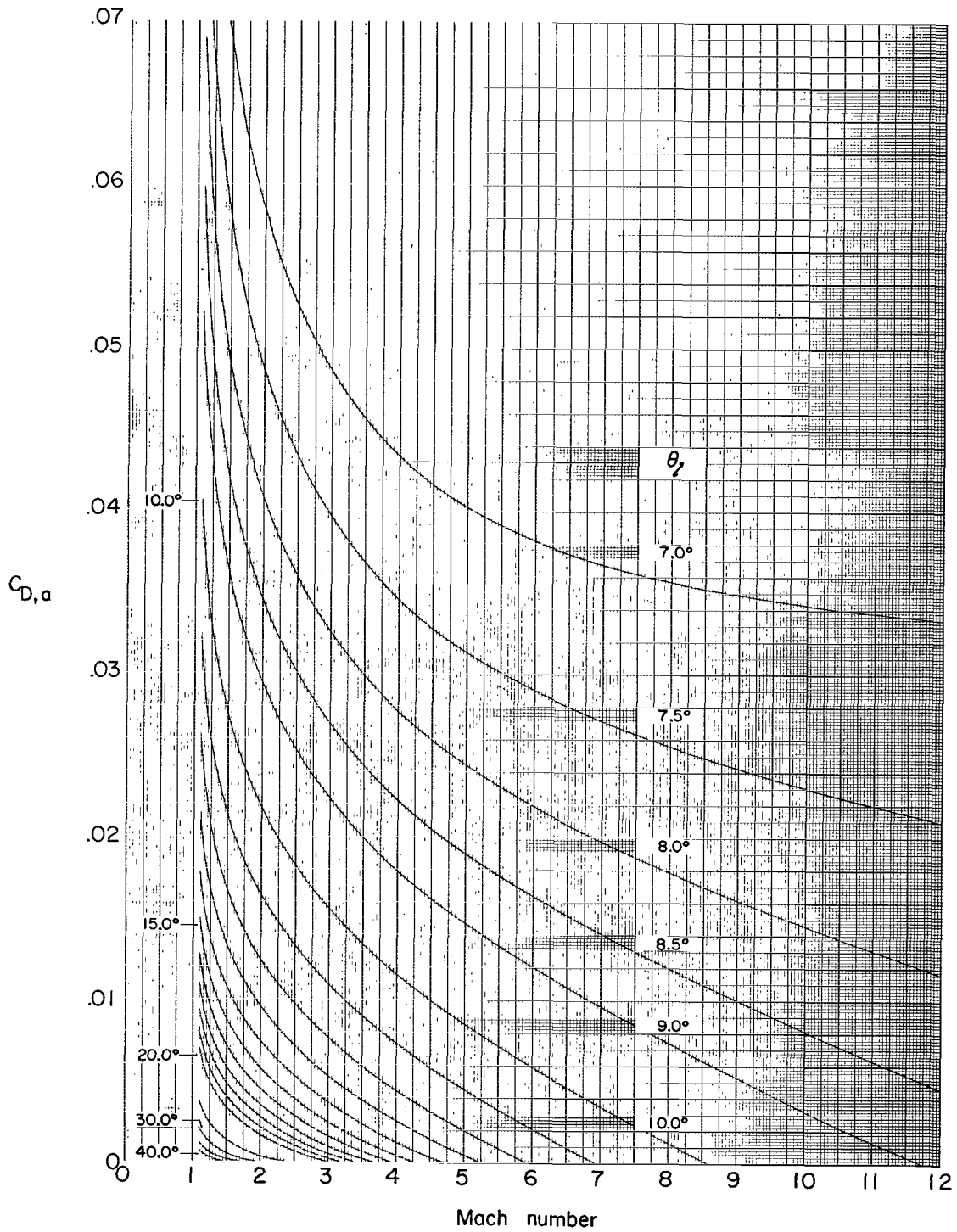
(b) Variation of mass-flow ratio with Mach number.

Figure 4.- Continued.



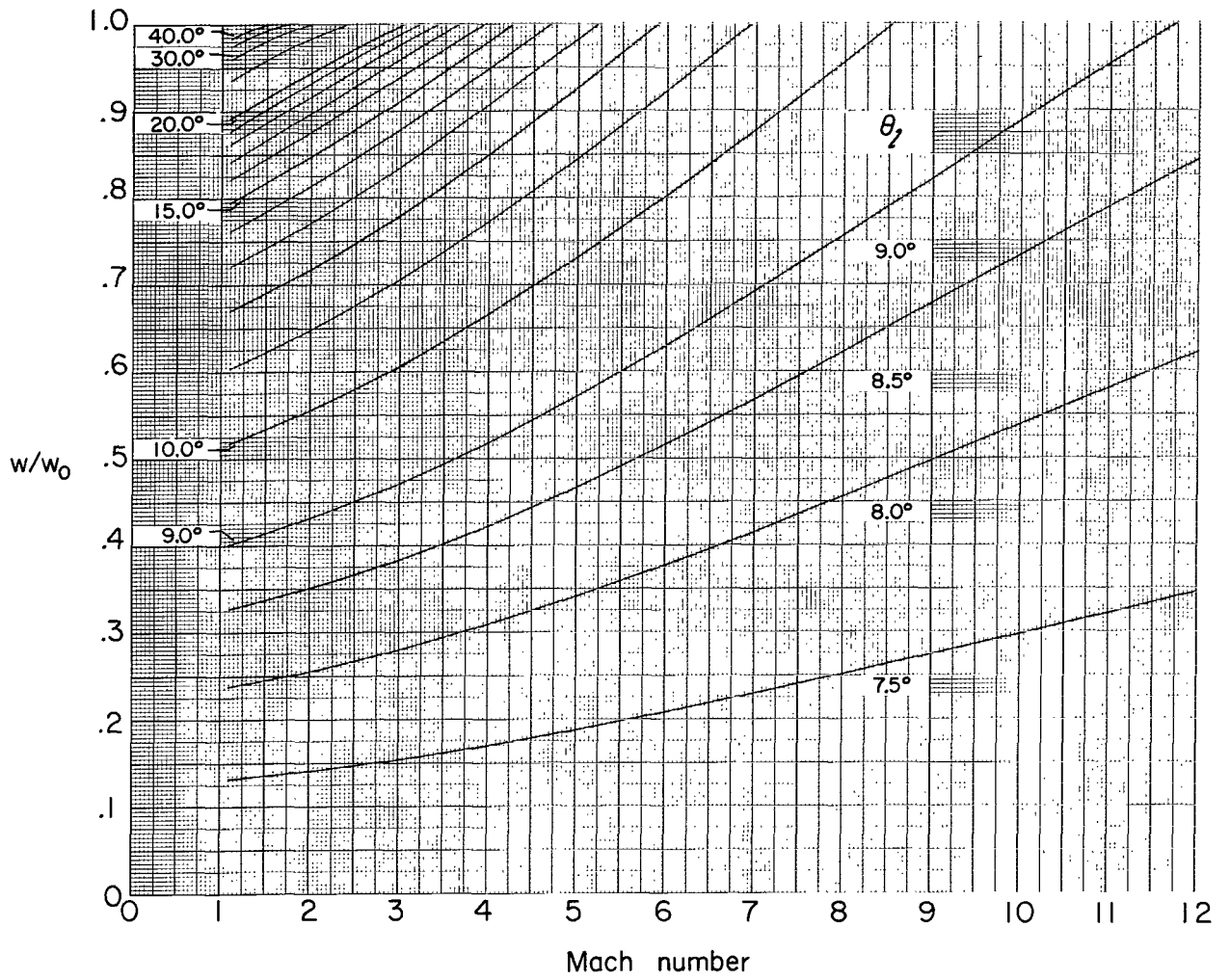
(c) Variation of additive drag with mass-flow ratio.

Figure 4.- Concluded.



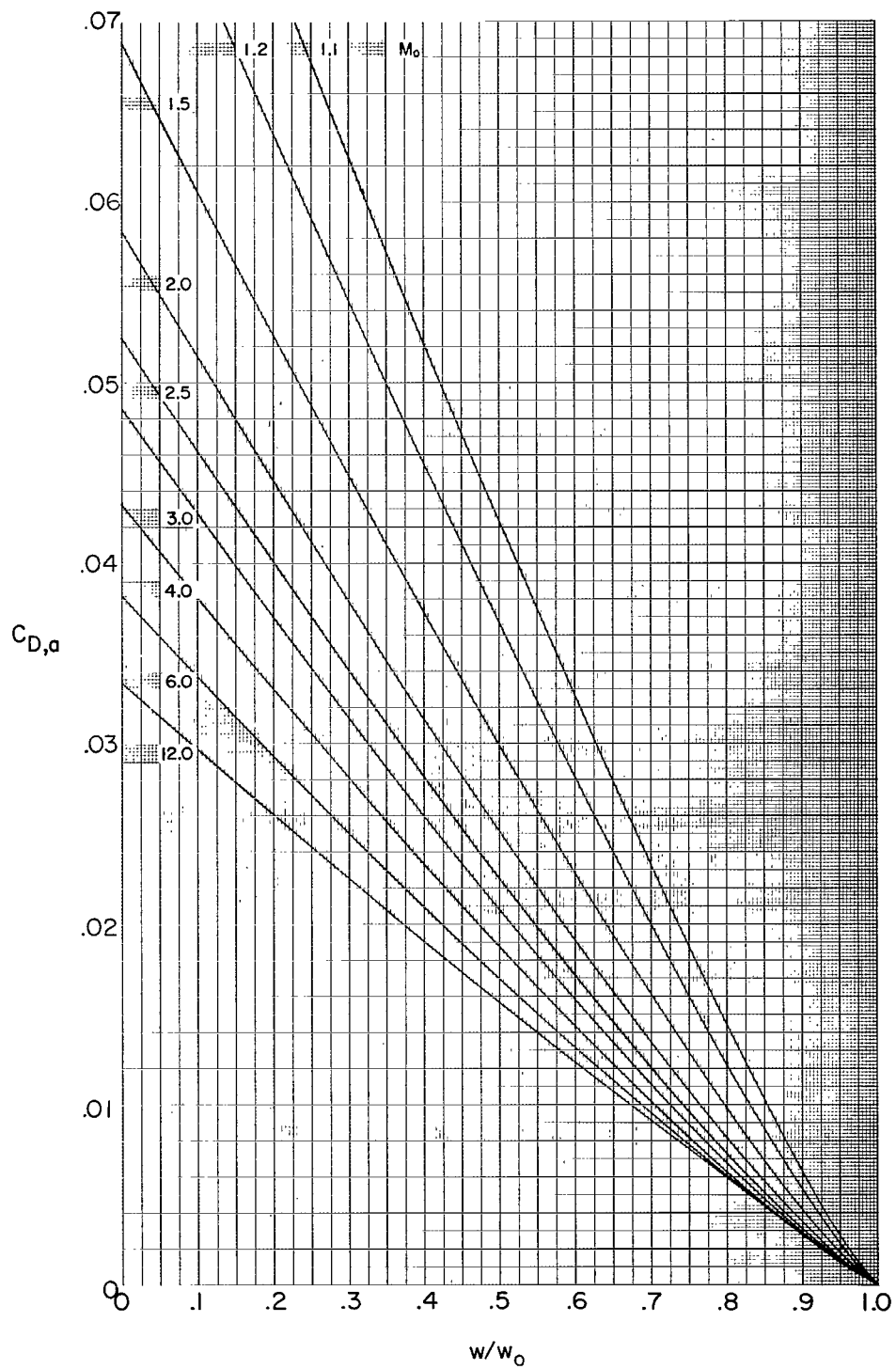
(a) Variation of additive drag with Mach number.

Figure 5.- Variation of additive drag and mass-flow ratio for  $\eta = 7^\circ$ .



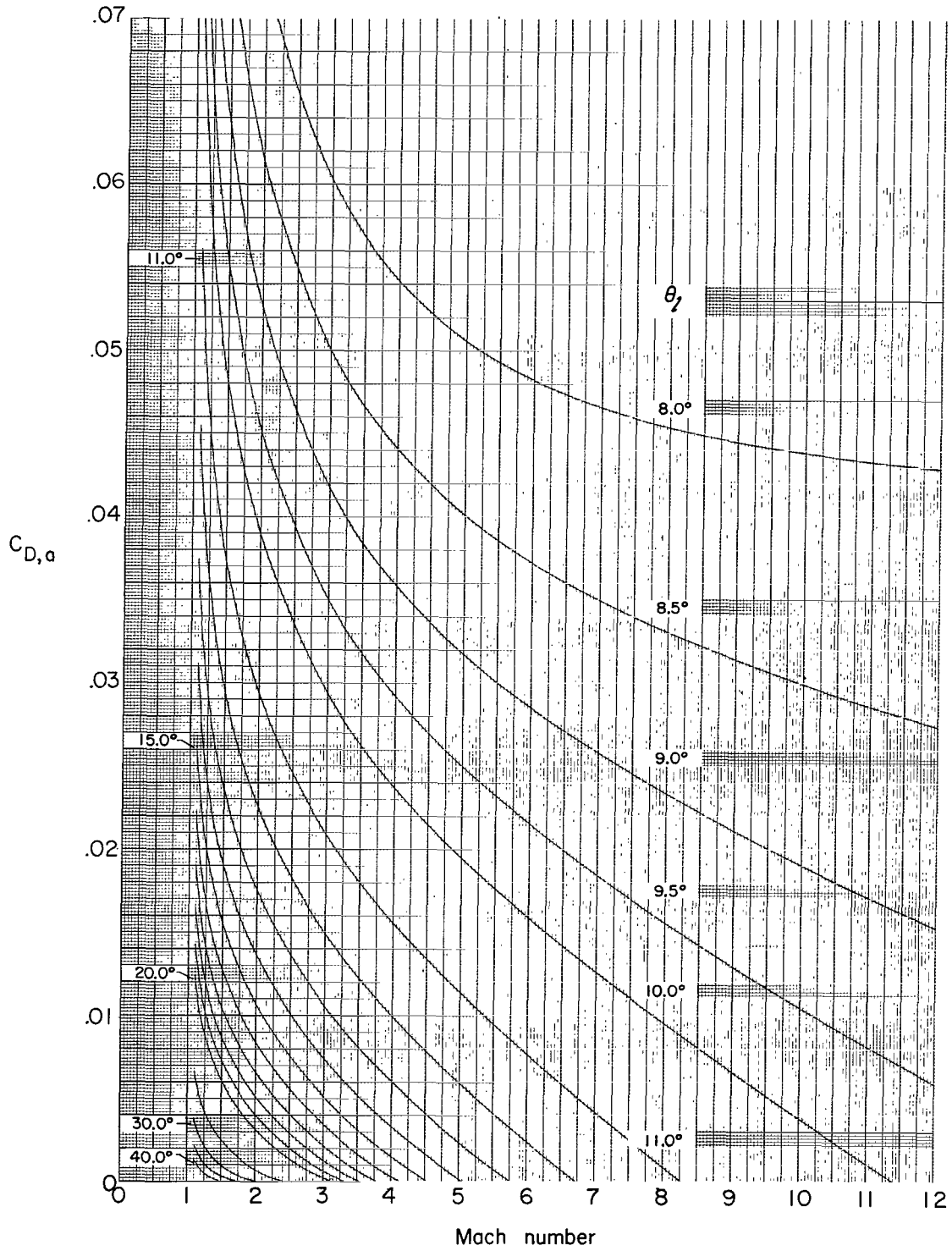
(b) Variation of mass-flow ratio with Mach number.

Figure 5.- Continued.



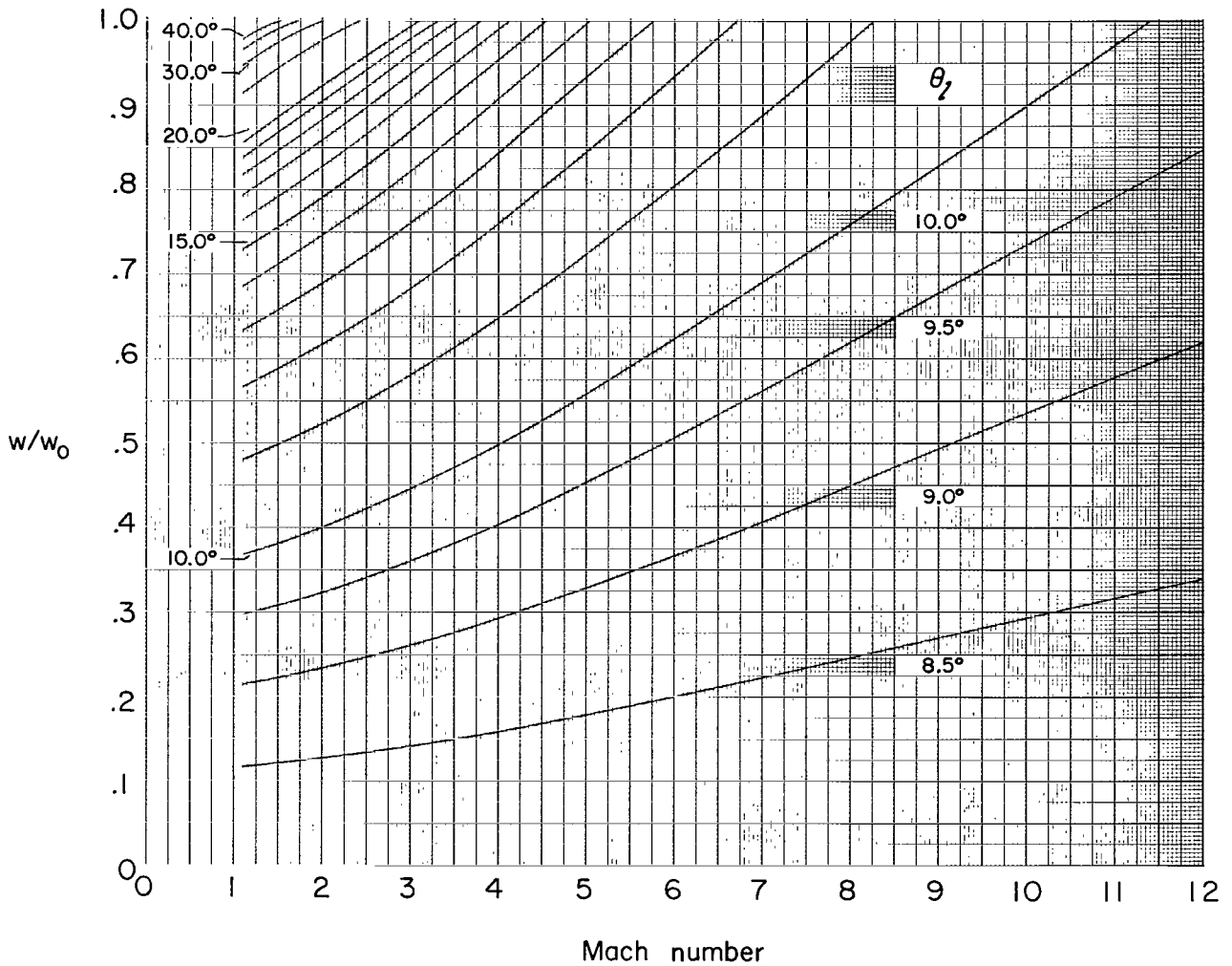
(c) Variation of additive drag with mass-flow ratio.

Figure 5.- Concluded.



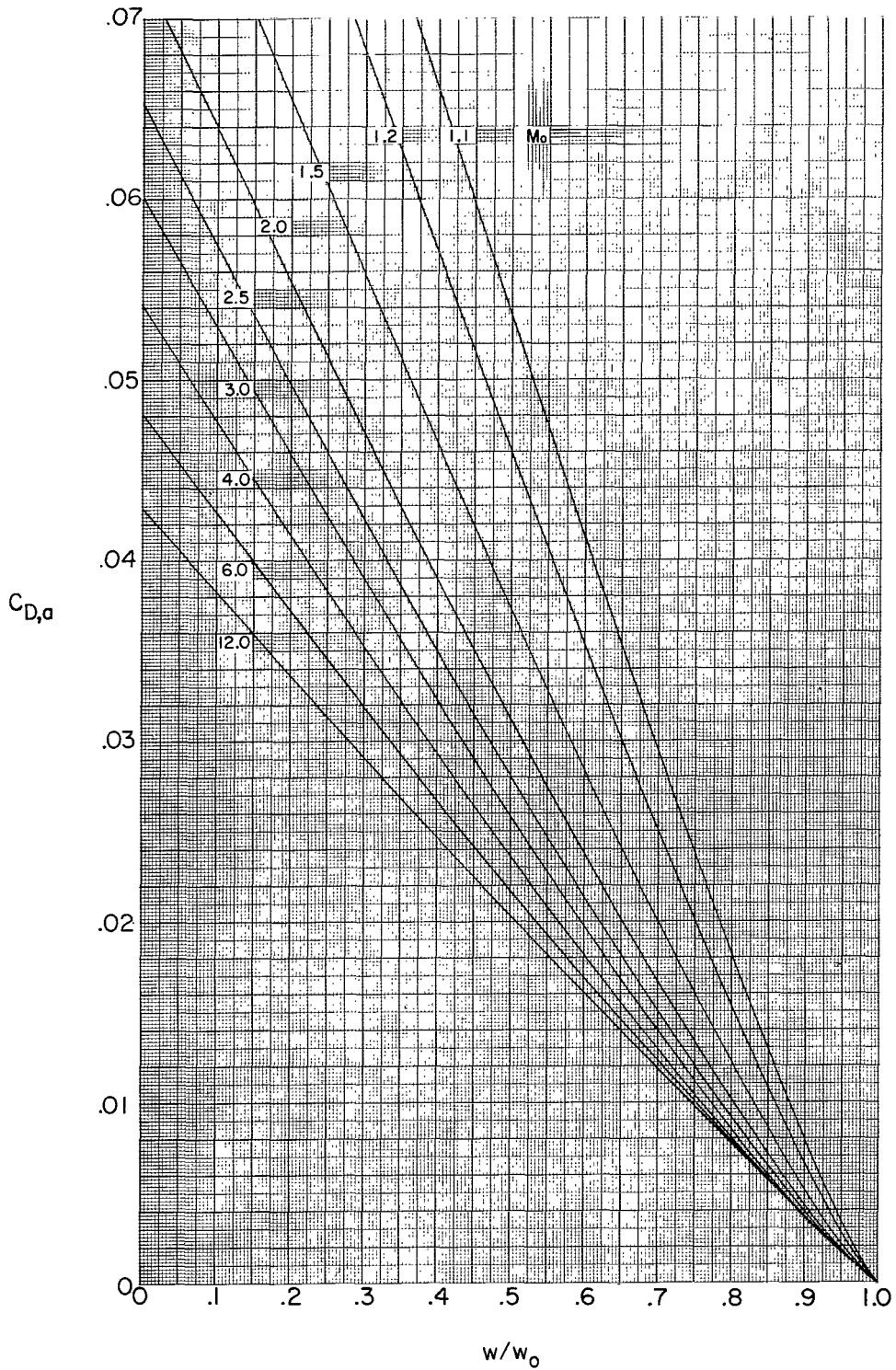
(a) Variation of additive drag with Mach number.

Figure 6.- Variation of additive drag and mass-flow ratio for  $\eta = 80$ .



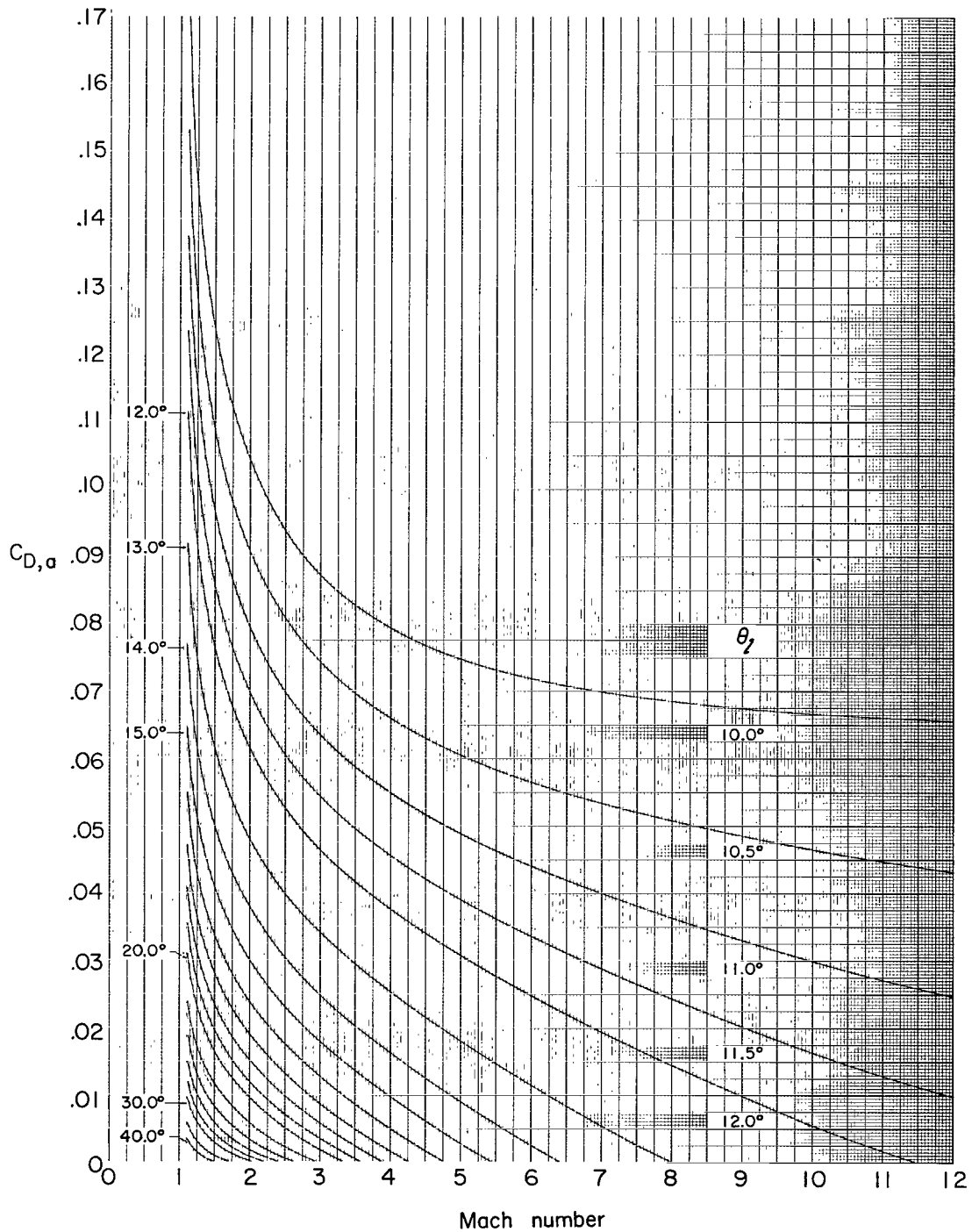
(b) Variation of mass-flow ratio with Mach number.

Figure 6.- Continued.



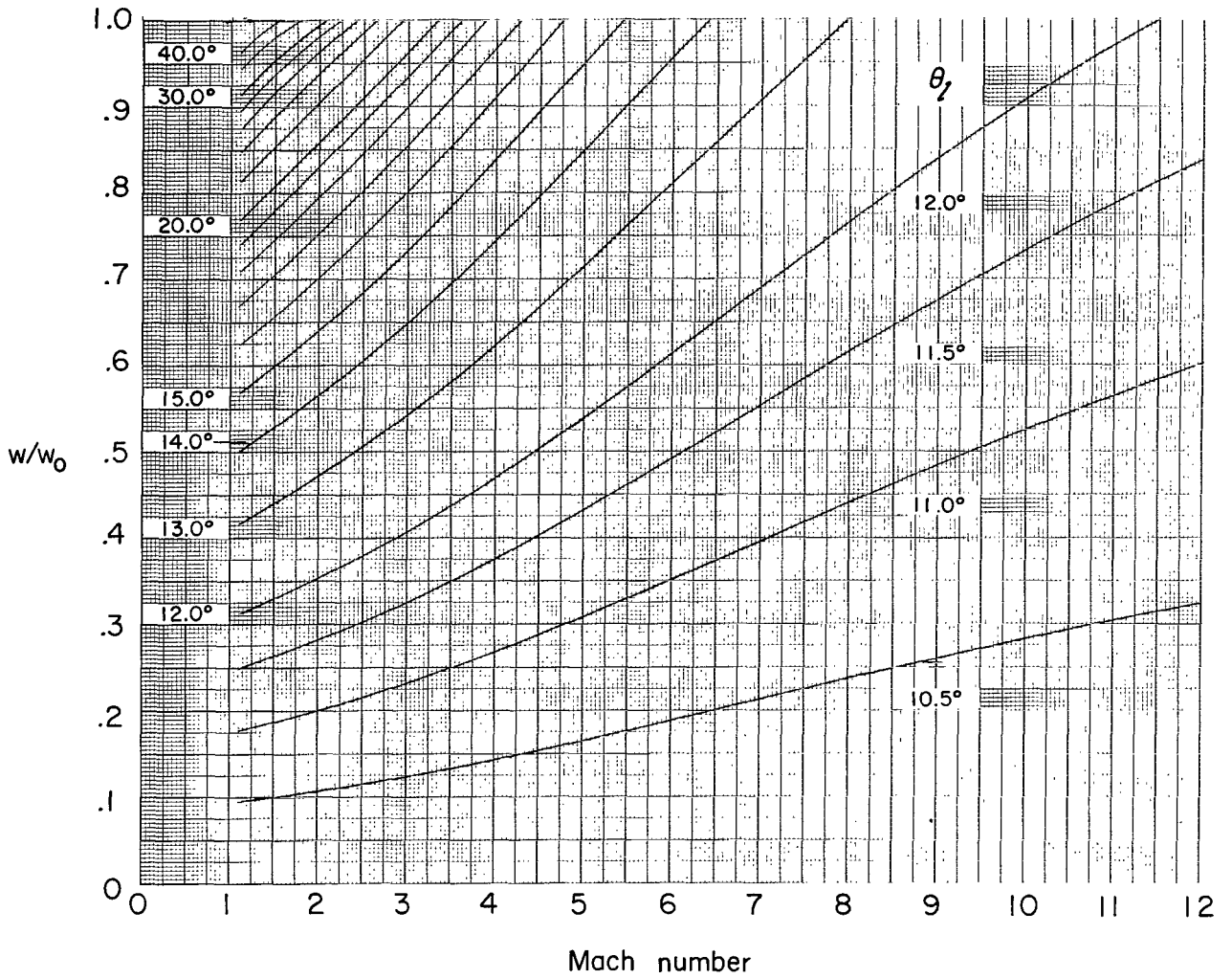
(c) Variation of additive drag with mass-flow ratio.

Figure 6.- Concluded.



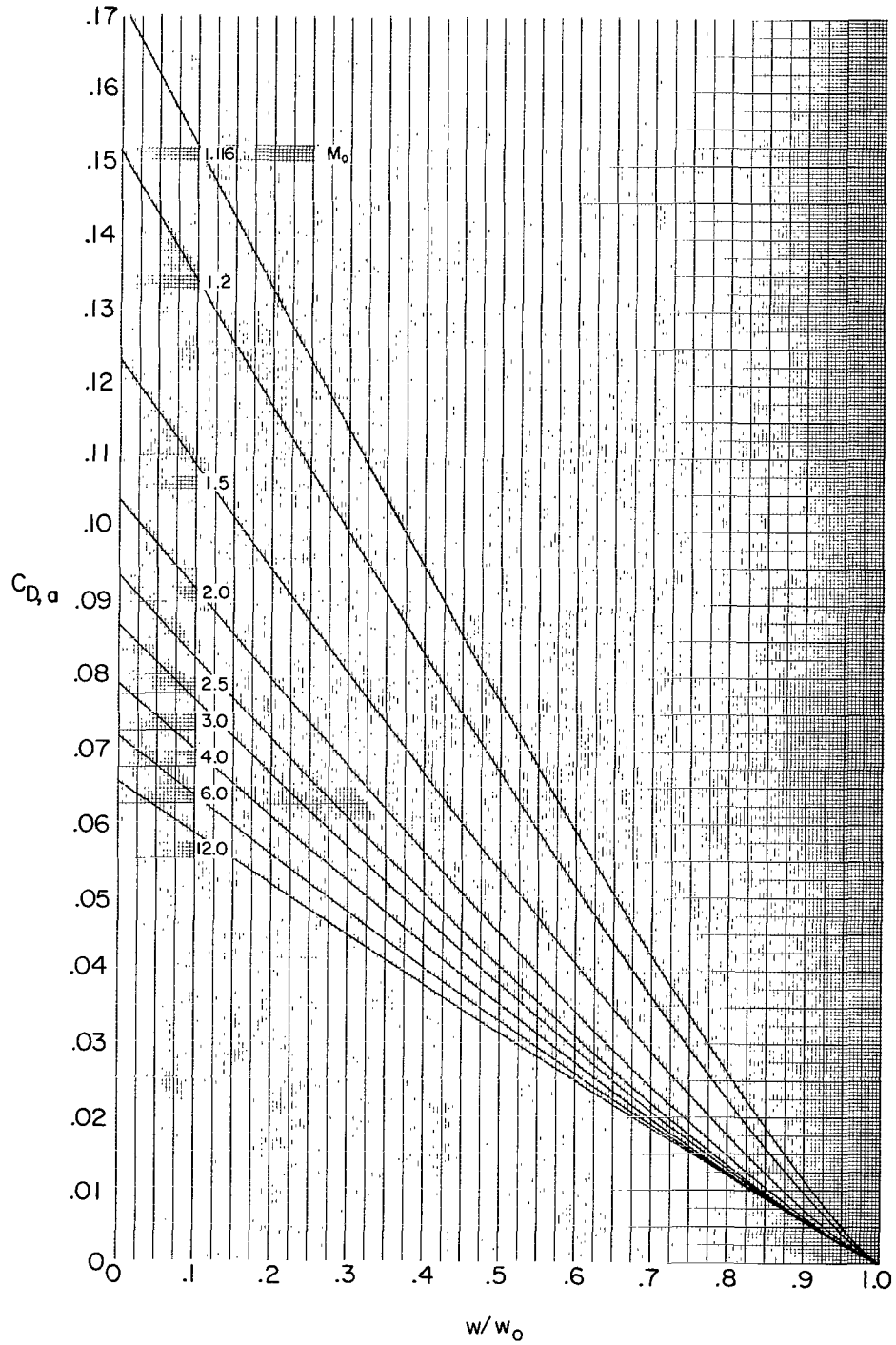
(a) Variation of additive drag with Mach number.

Figure 7.- Variation of additive drag and mass-flow ratio for  $\eta = 100^\circ$ .



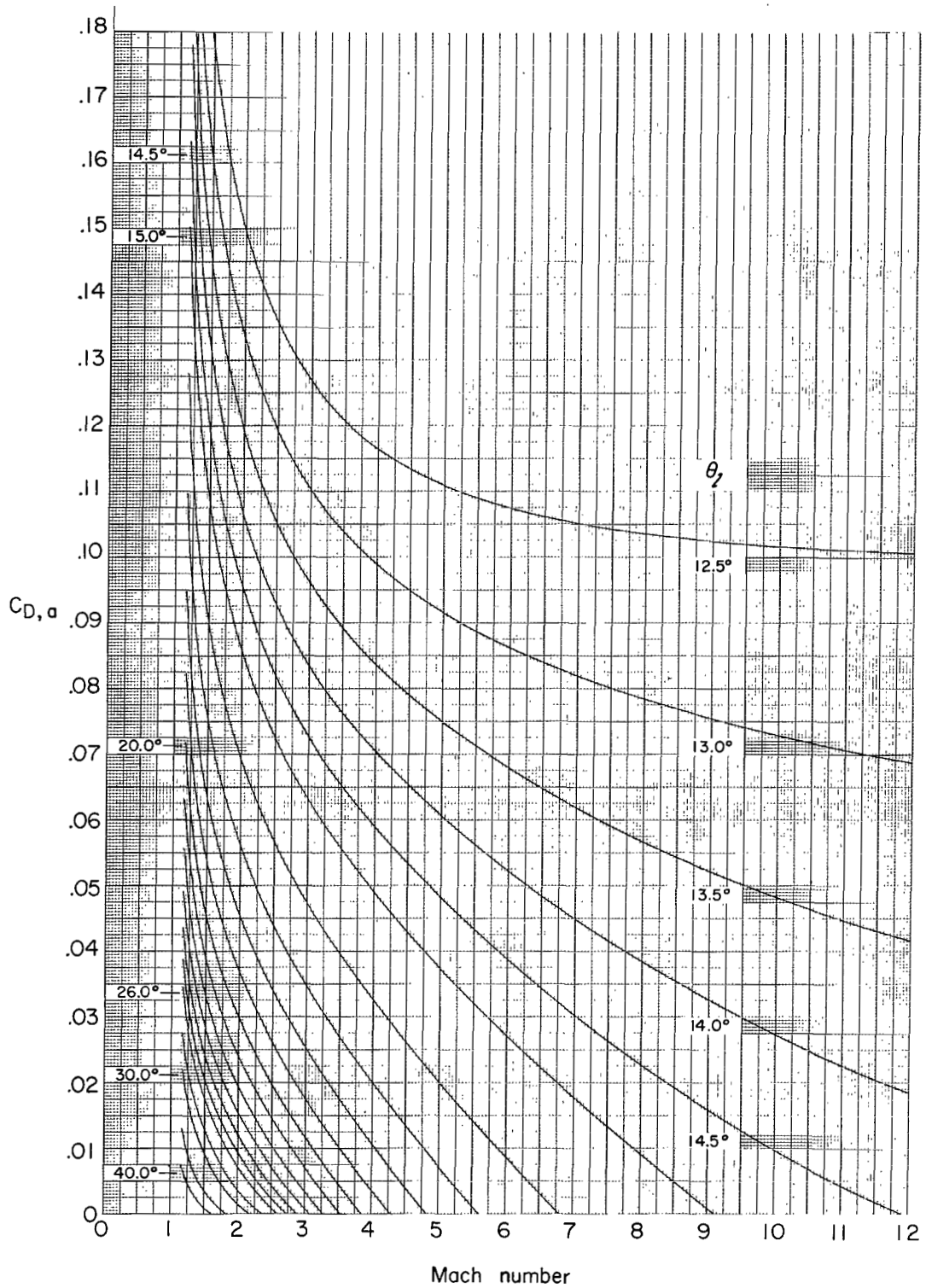
(b) Variation of mass-flow ratio with Mach number.

Figure 7.- Continued.



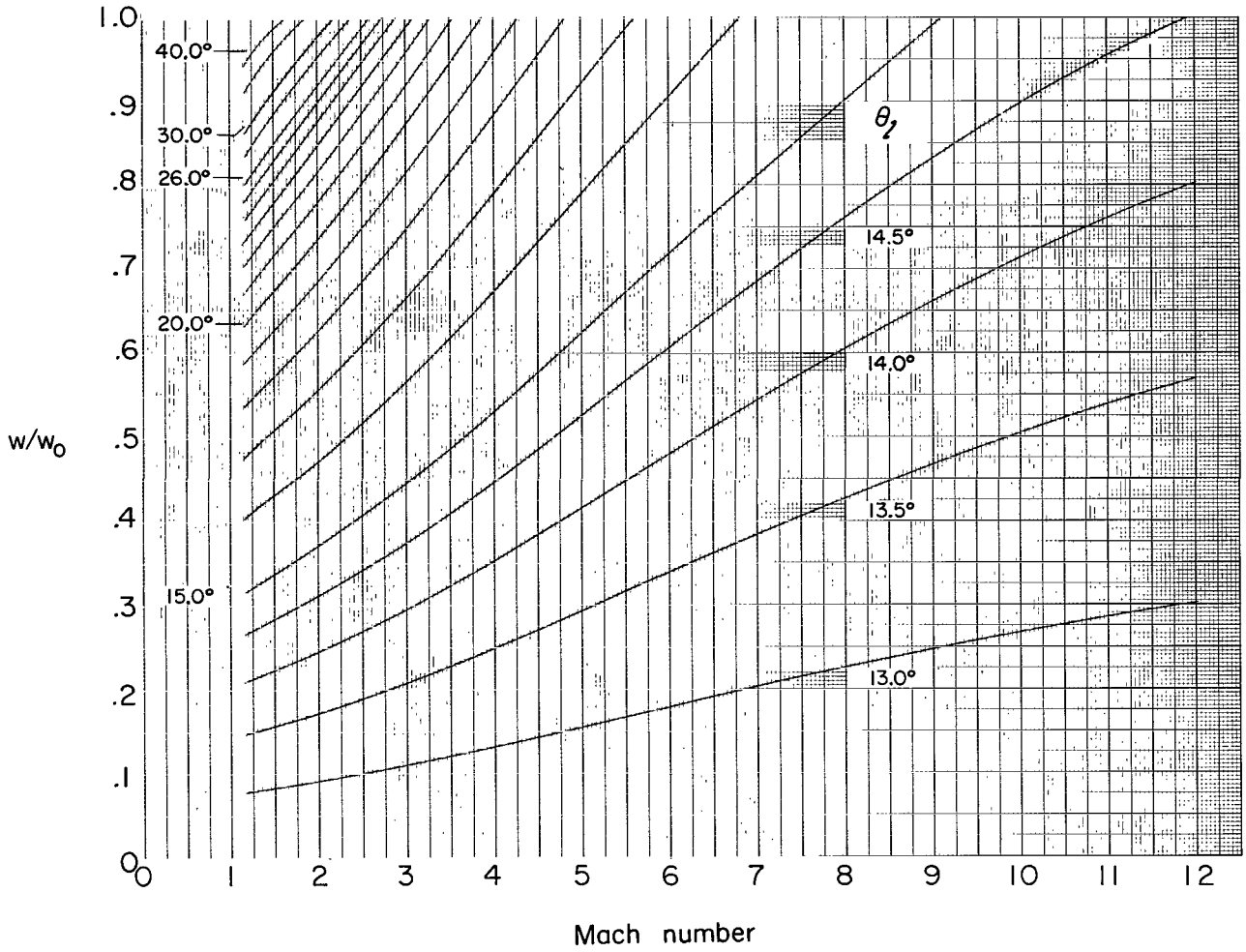
(c) Variation of additive drag with mass-flow ratio.

Figure 7.- Concluded.



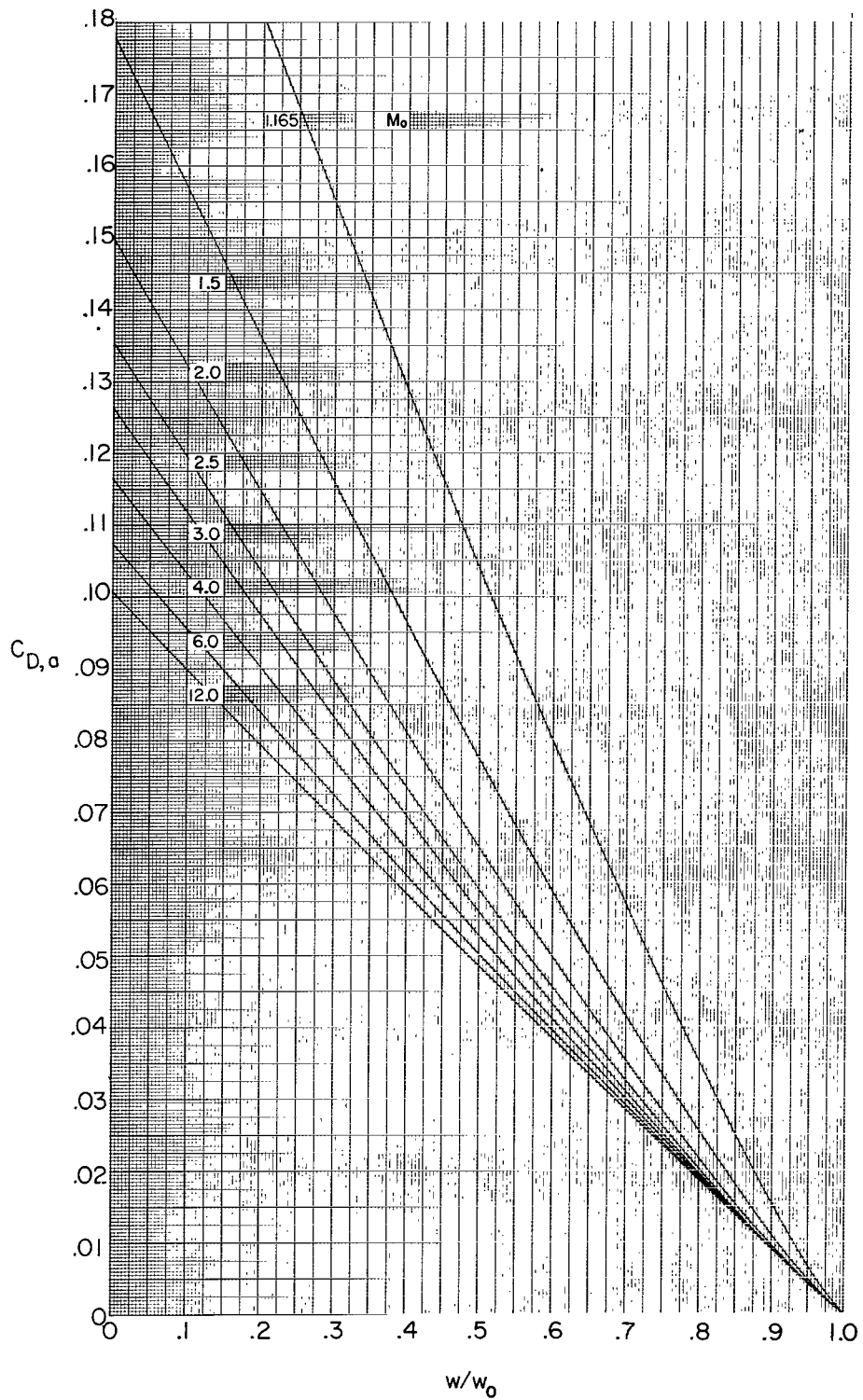
(a) Variation of additive drag with Mach number.

Figure 8.- Variation of additive drag and mass-flow ratio for  $\eta = 12.5^\circ$ .



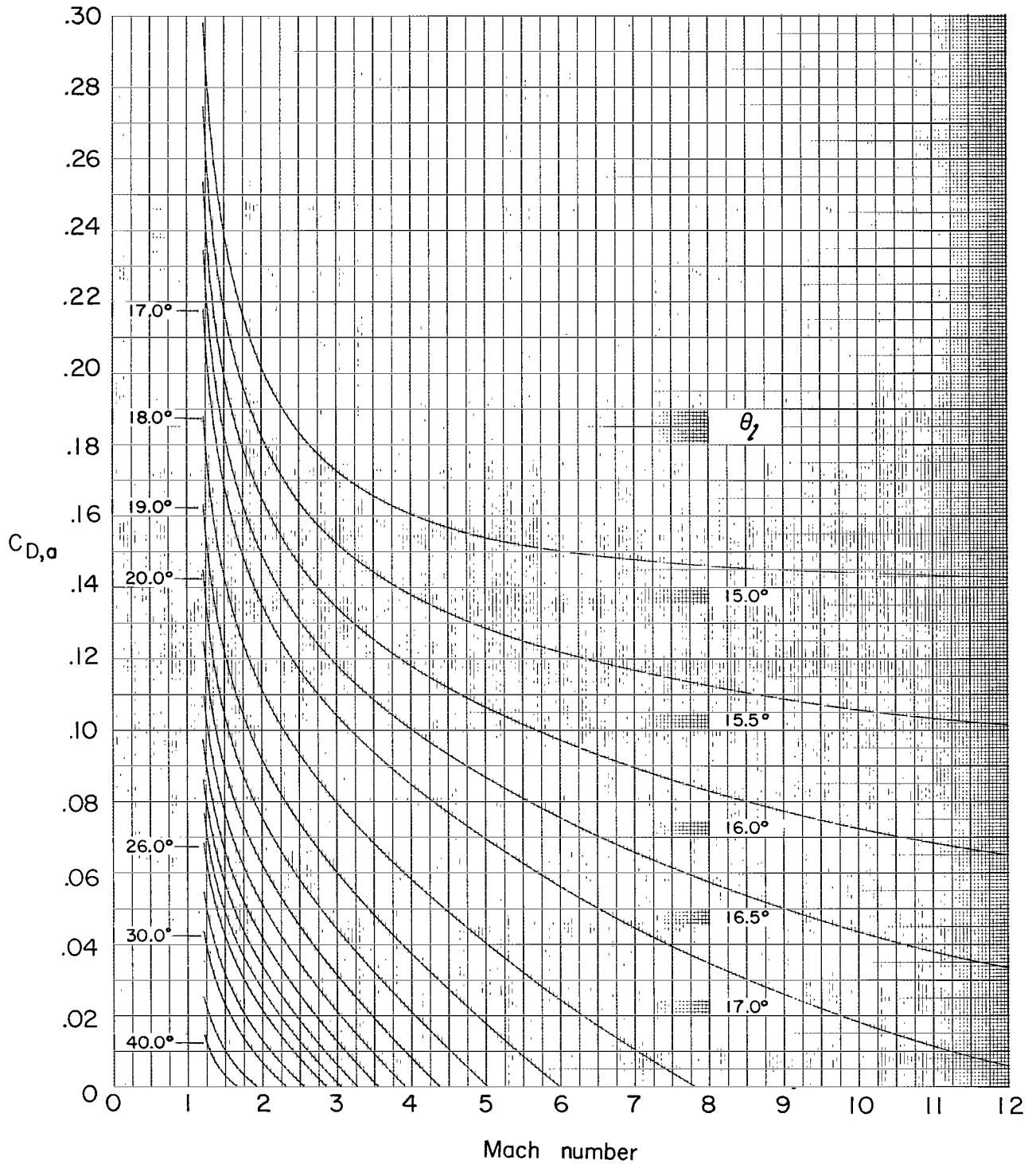
(b) Variation of mass-flow ratio with Mach number.

Figure 8.- Continued.



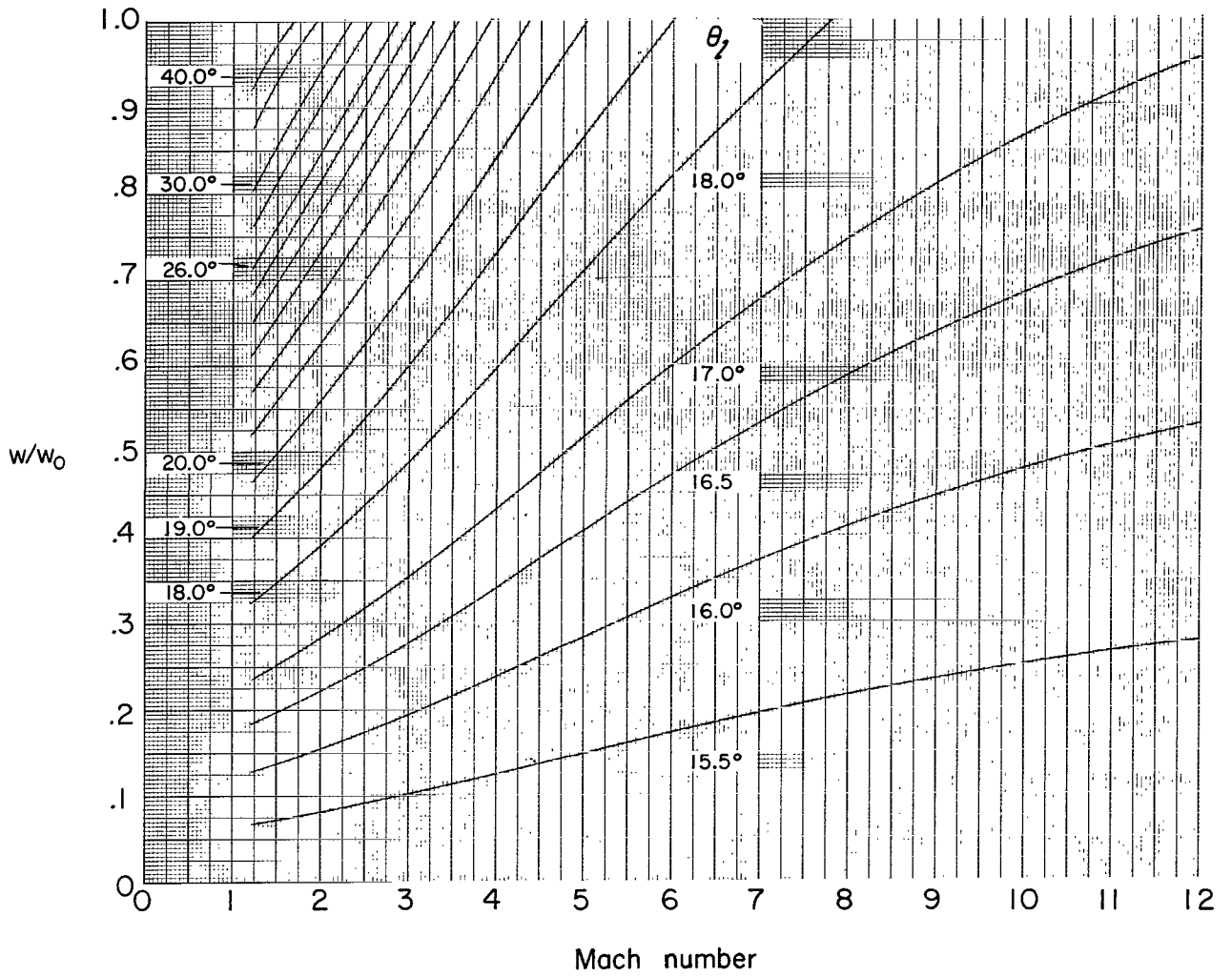
(c) Variation of additive drag with mass-flow ratio.

Figure 8.- Concluded.



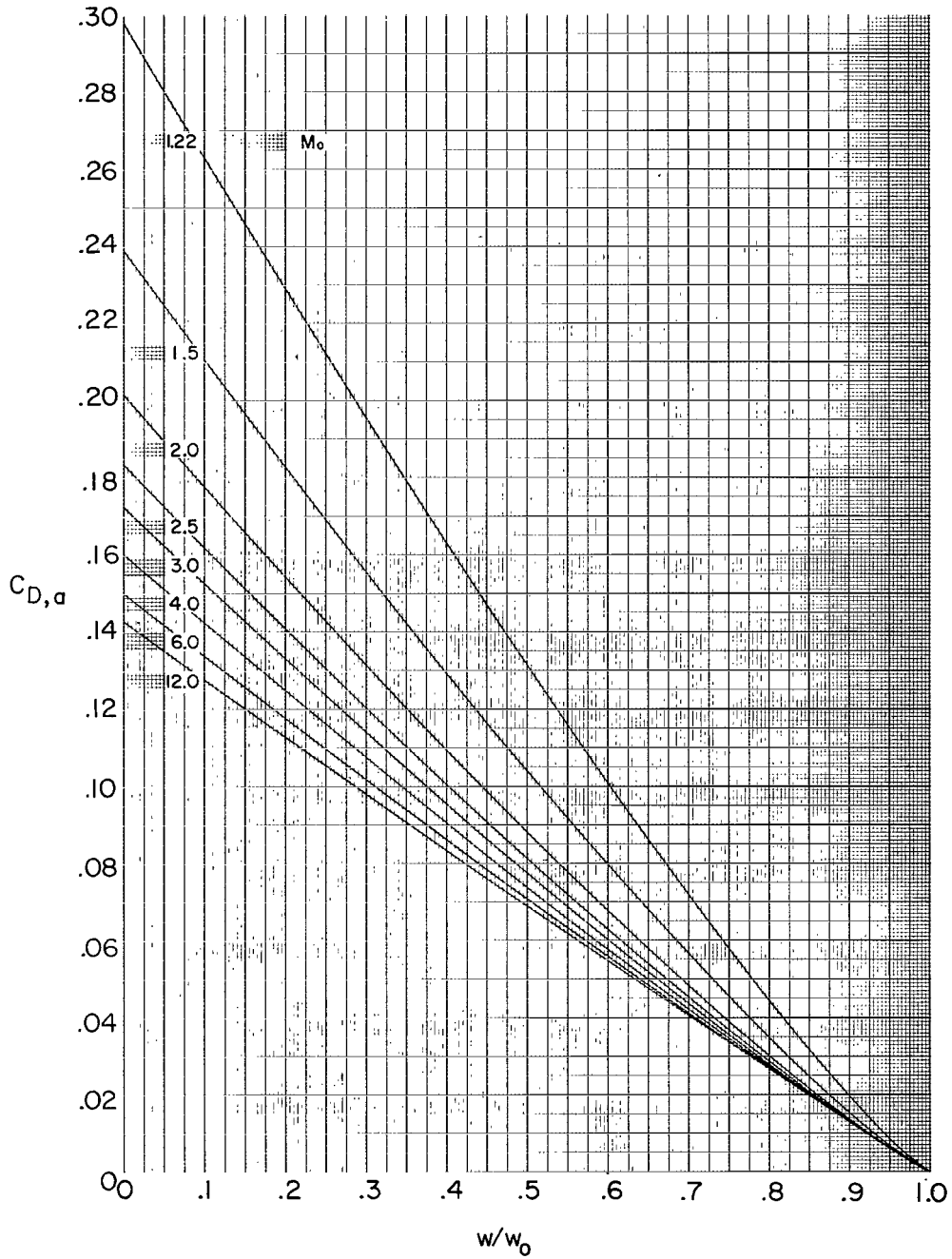
(a) Variation of additive drag with Mach number.

Figure 9.- Variation of additive drag and mass-flow ratio for  $\eta = 15^\circ$ .



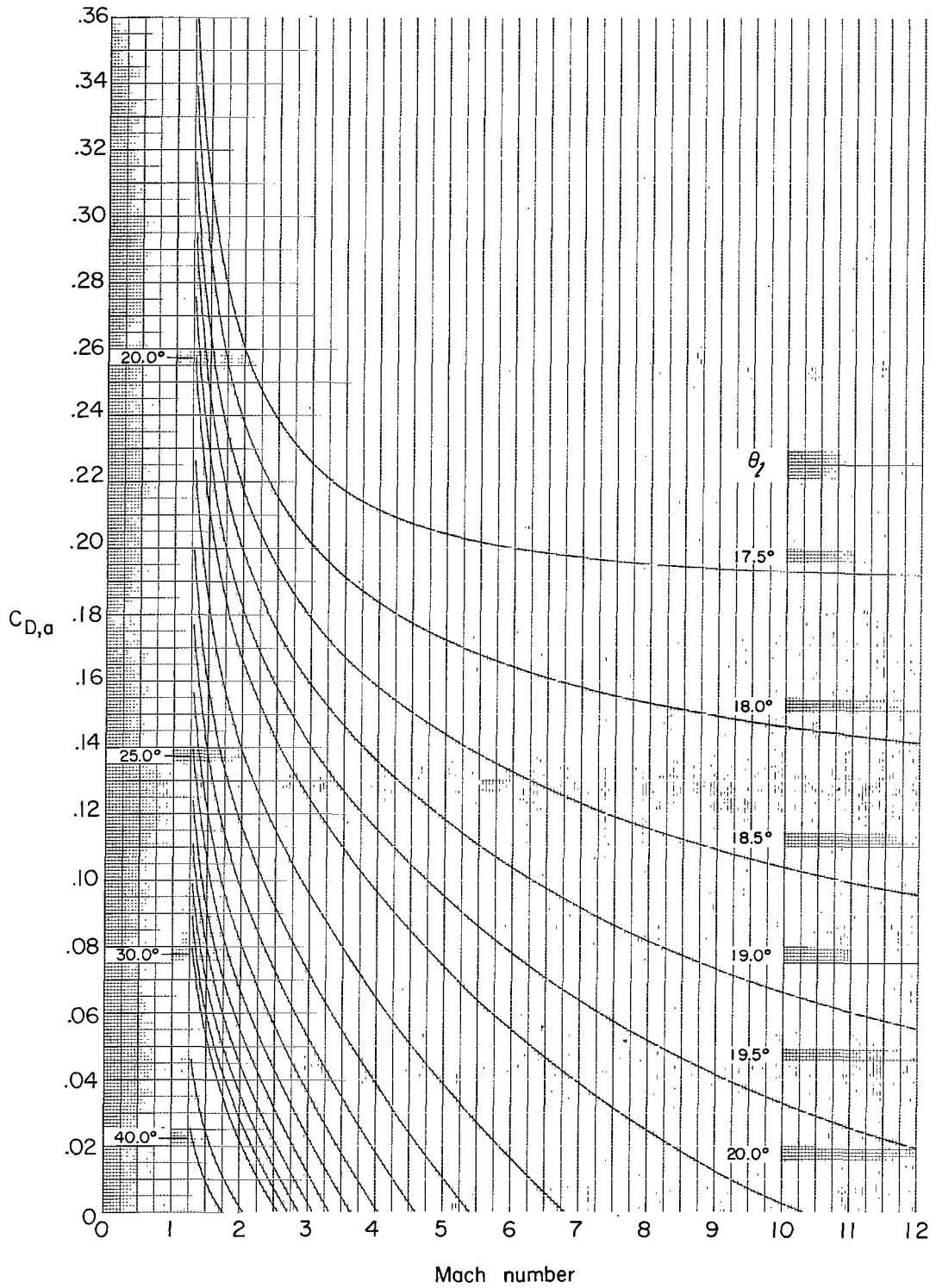
(b) Variation of mass-flow ratio with Mach number.

Figure 9.- Continued.



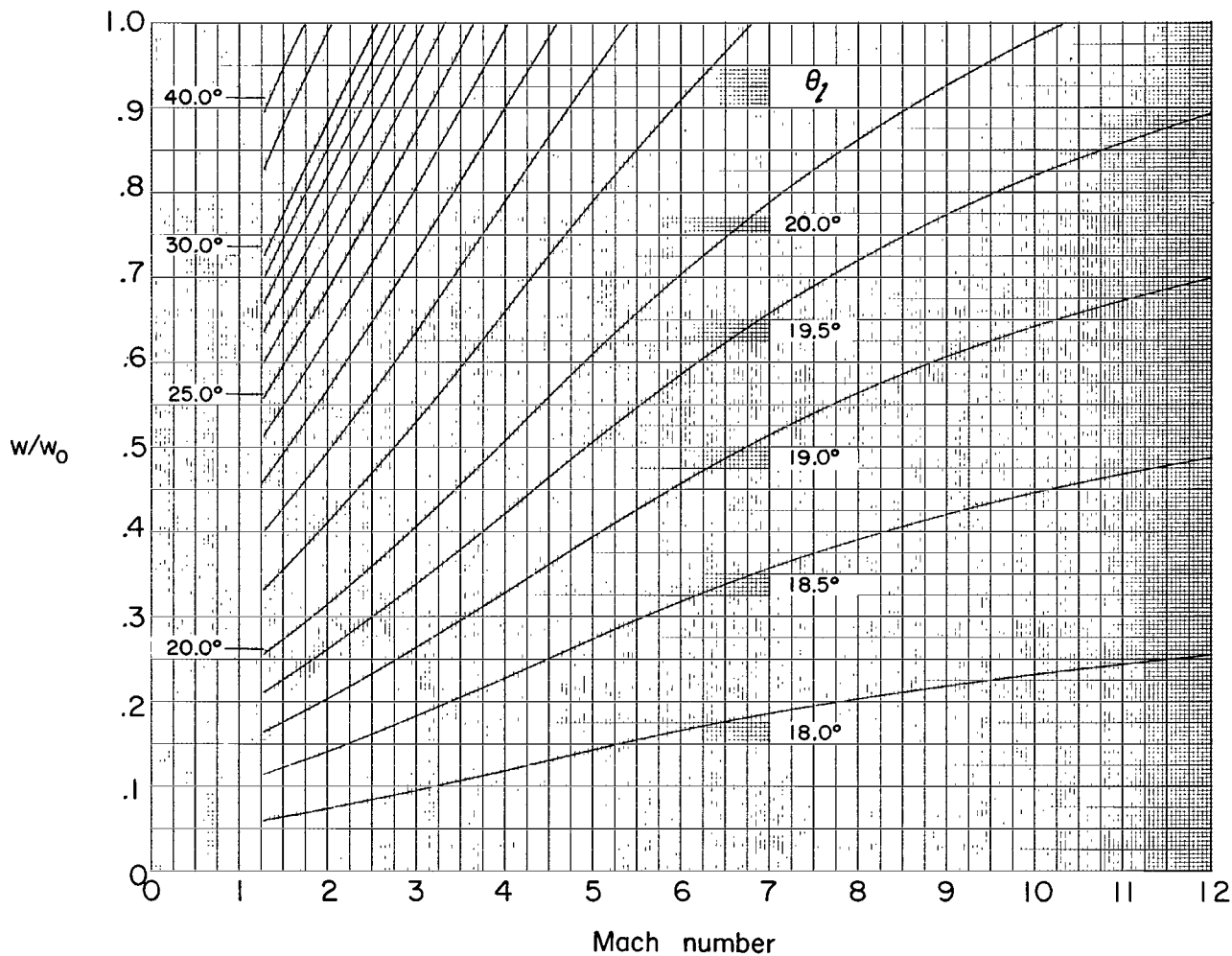
(c) Variation of additive drag with mass-flow ratio.

Figure 9.- Concluded.



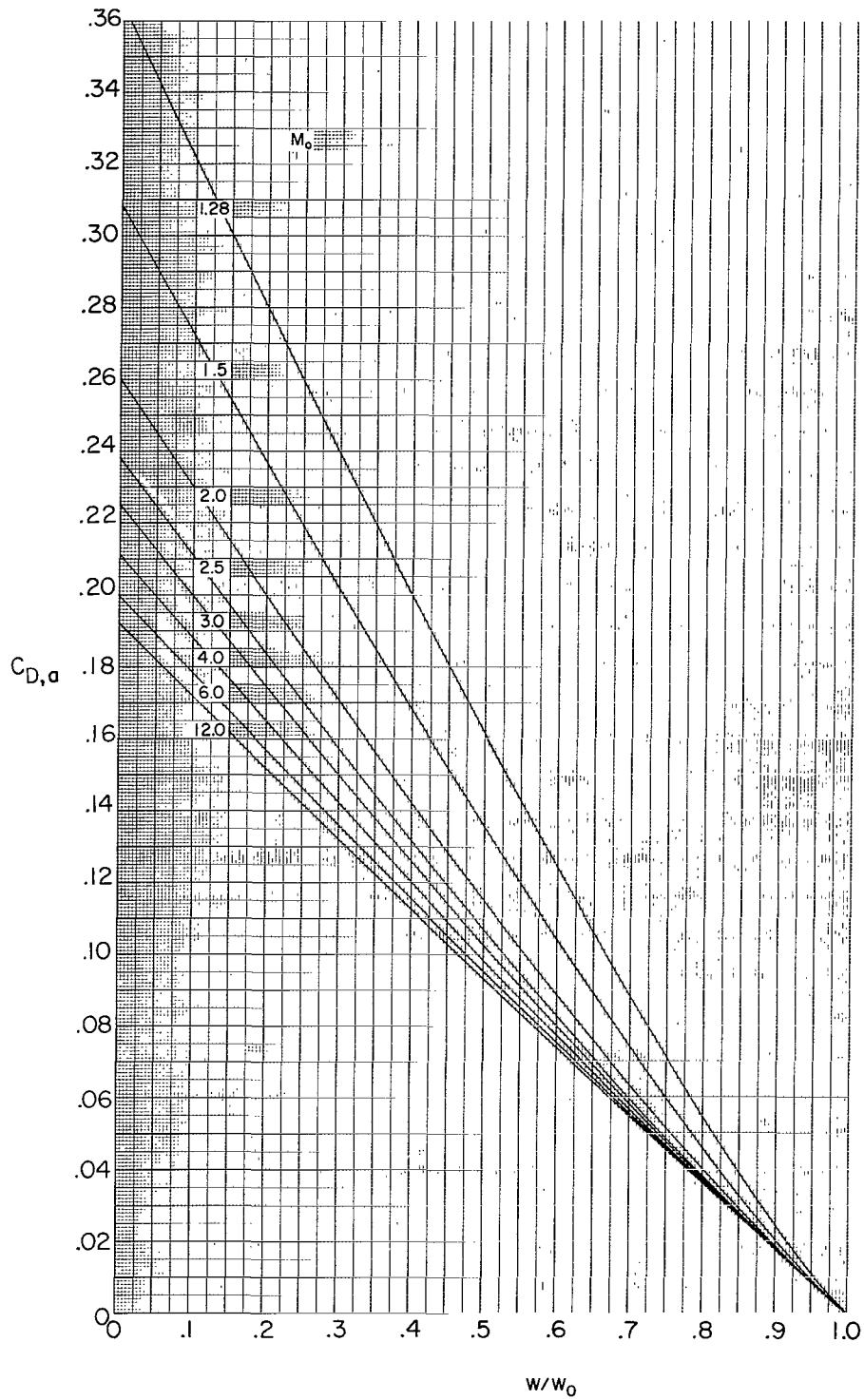
(a) Variation of additive drag with Mach number.

Figure 10.- Variation of additive drag and mass-flow ratio for  $\eta = 17.5^\circ$ .



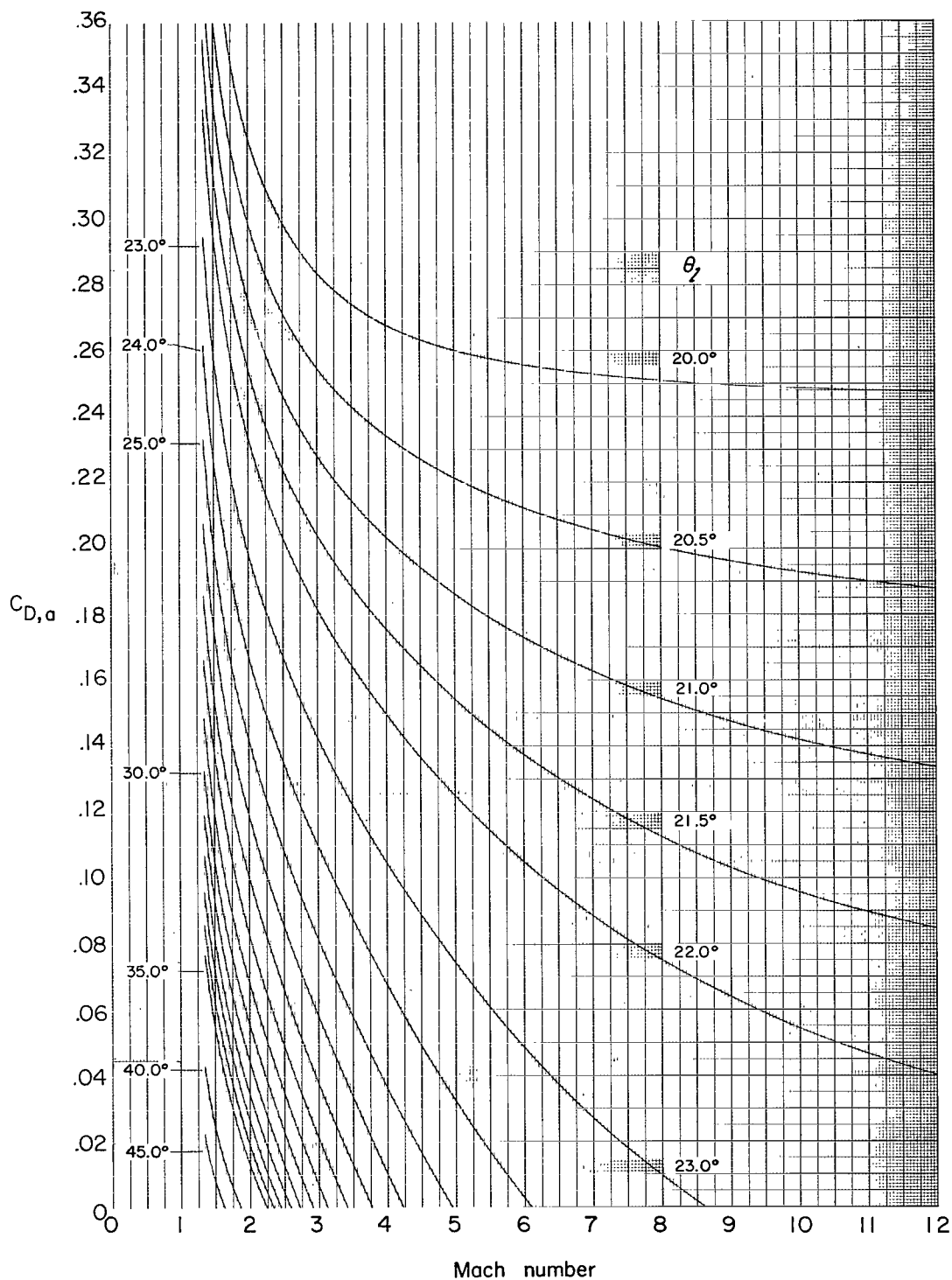
(b) Variation of mass-flow ratio with Mach number.

Figure 10.- Continued.



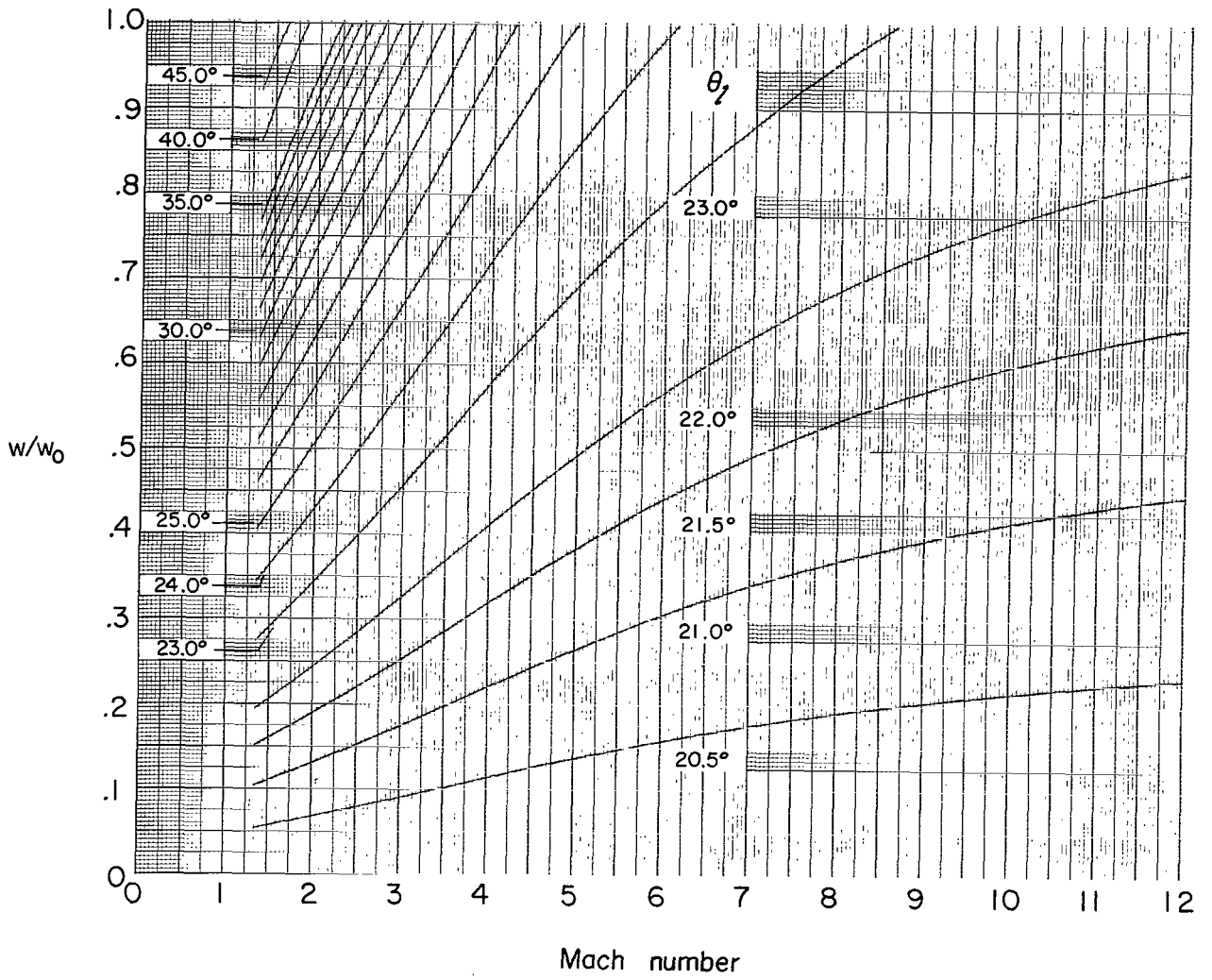
(c) Variation of additive drag with mass-flow ratio.

Figure 10.- Concluded.



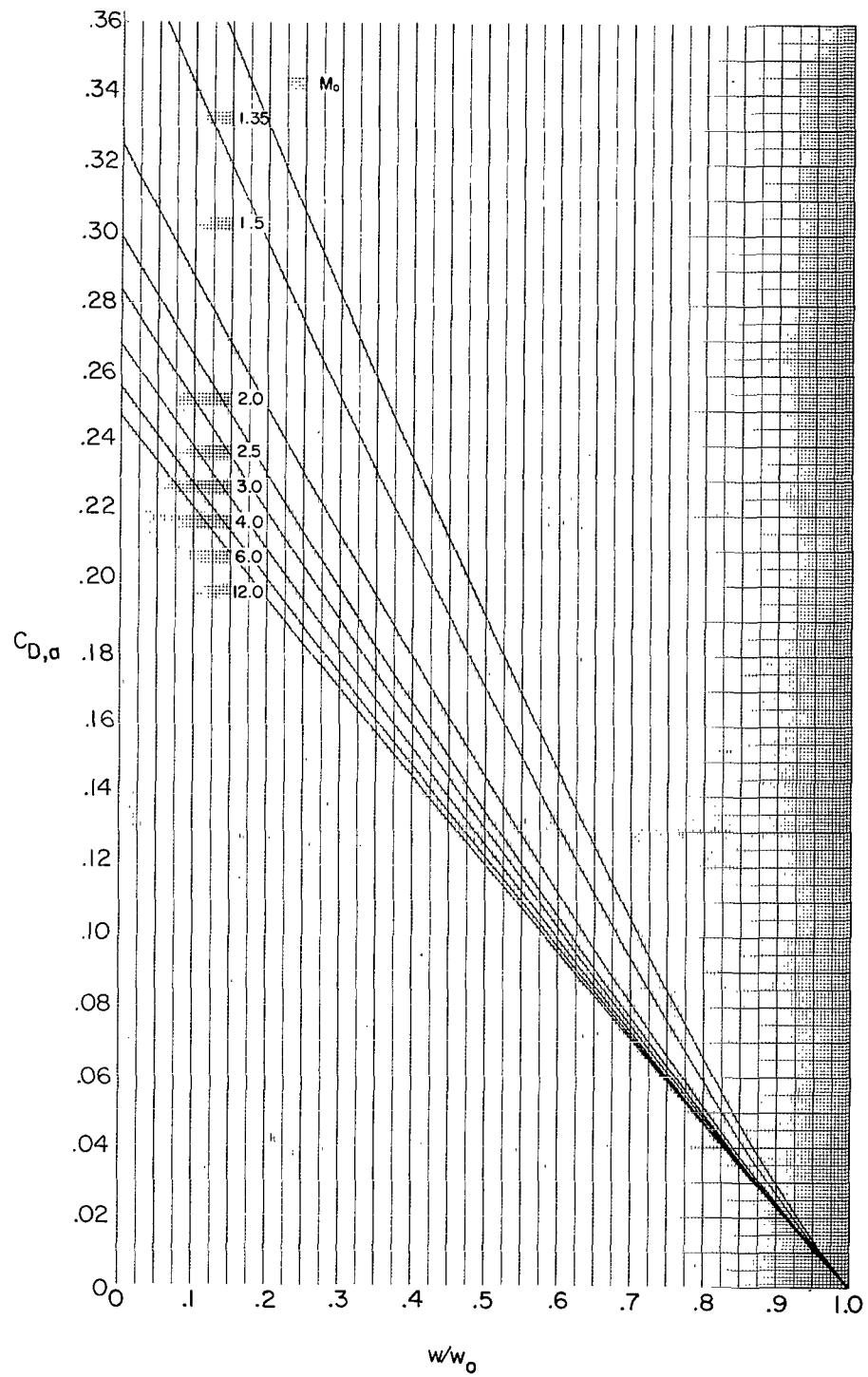
(a) Variation of additive drag with Mach number.

Figure 11.- Variation of additive drag and mass-flow ratio for  $\eta = 20^\circ$ .



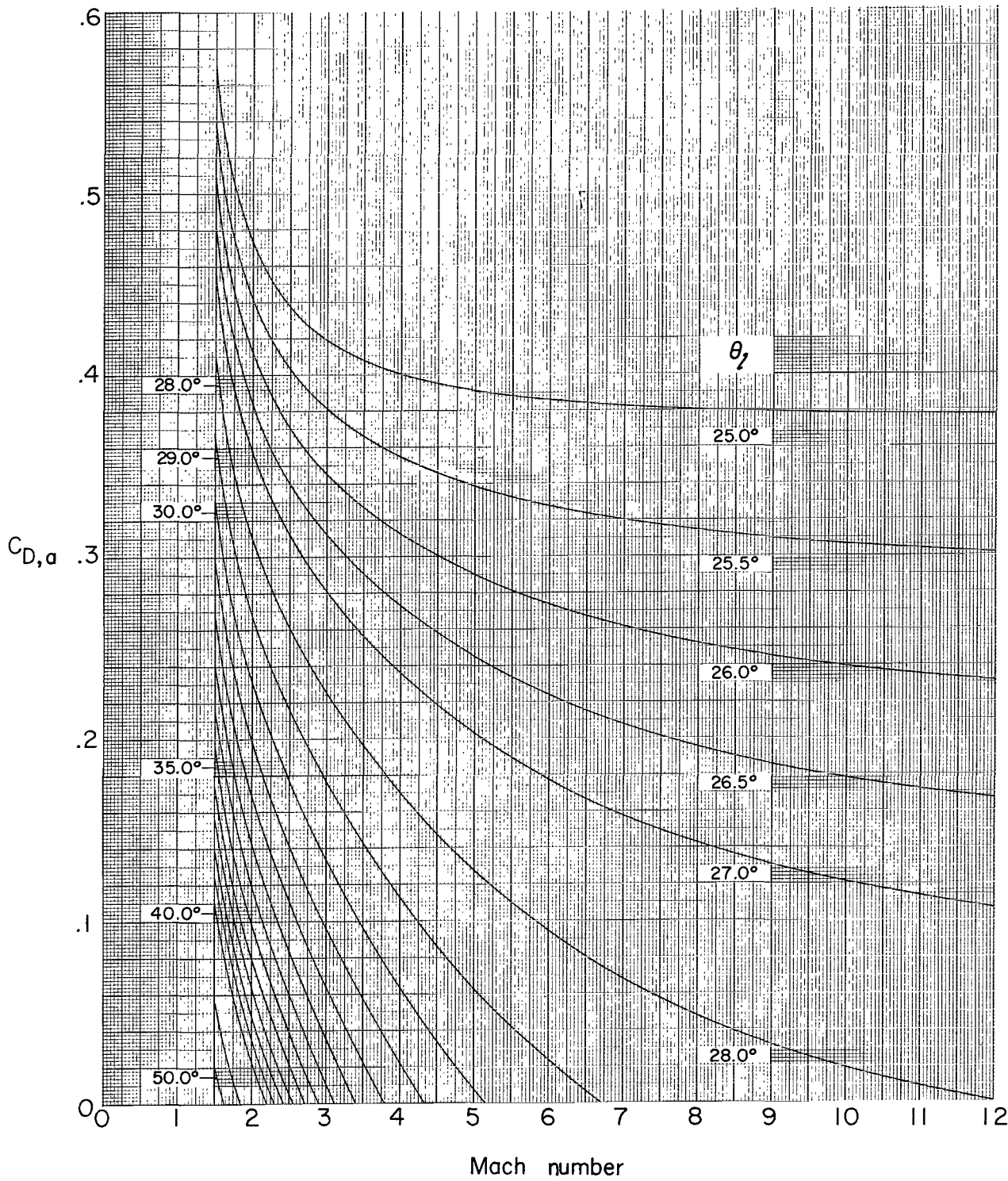
(b) Variation of mass-flow ratio with Mach number.

Figure 11.- Continued.



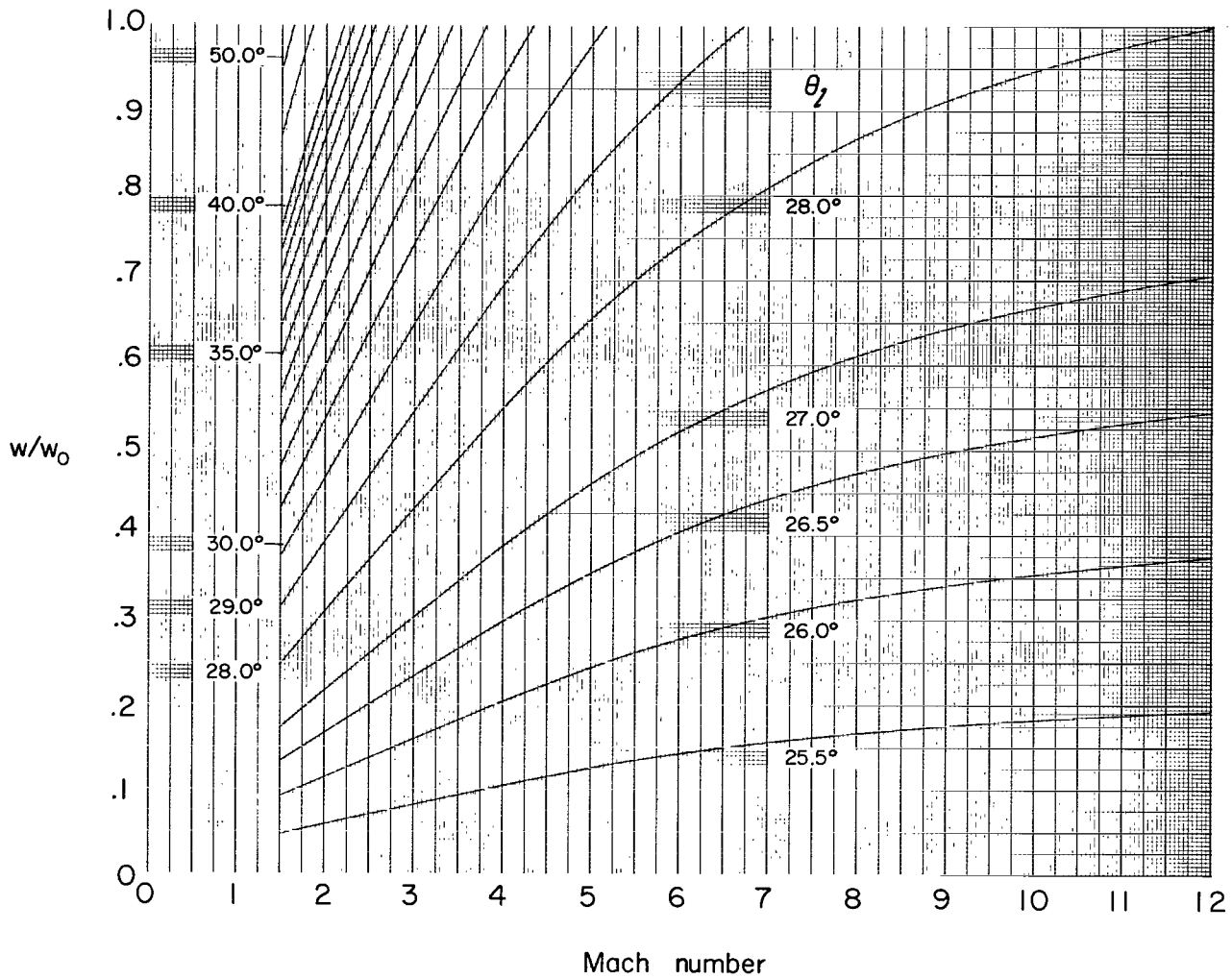
(c) Variation of additive drag with mass-flow ratio.

Figure 11.- Concluded.



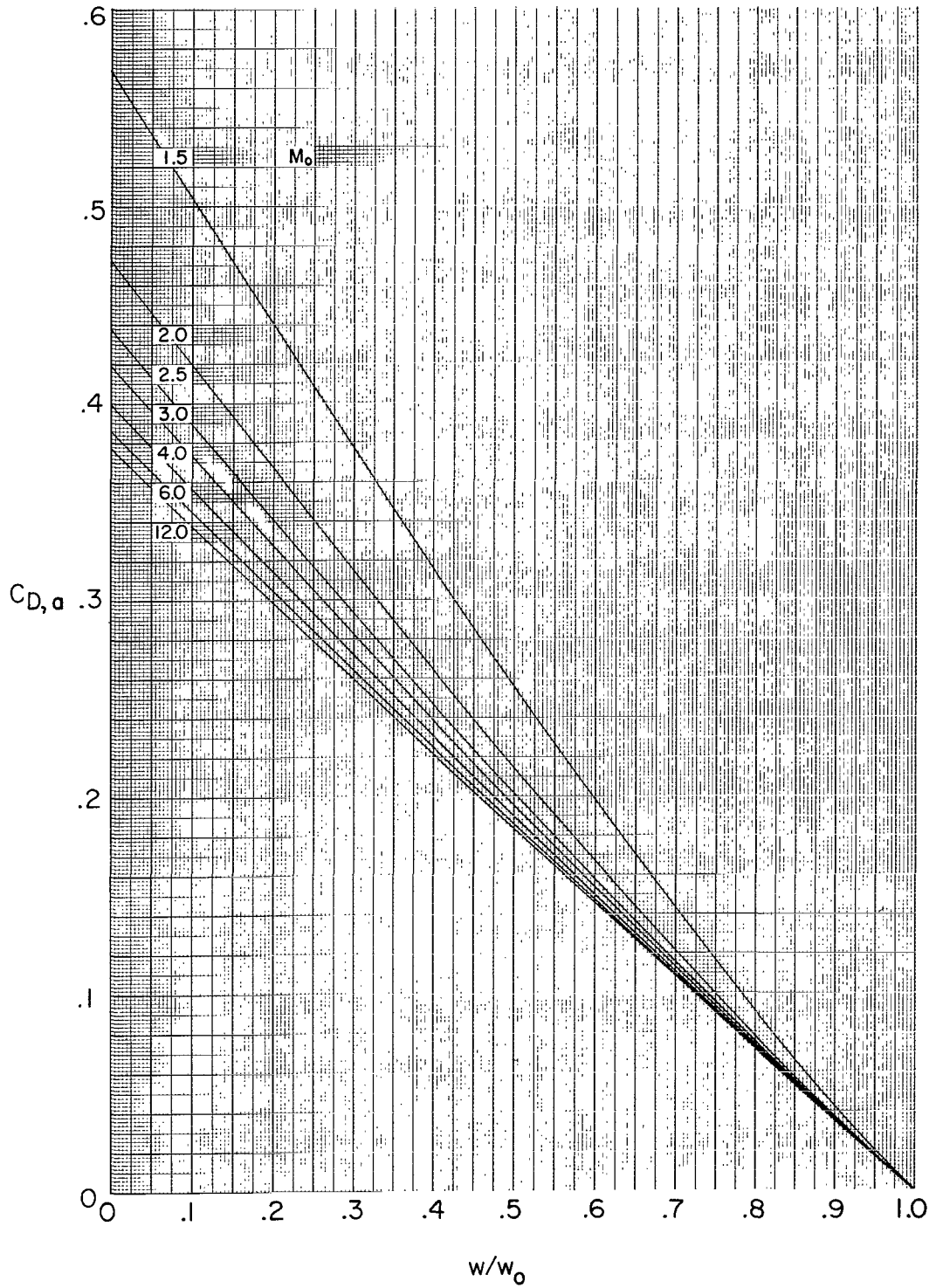
(a) Variation of additive drag with Mach number.

Figure 12.- Variation of additive drag and mass-flow ratio for  $\eta = 25^\circ$ .



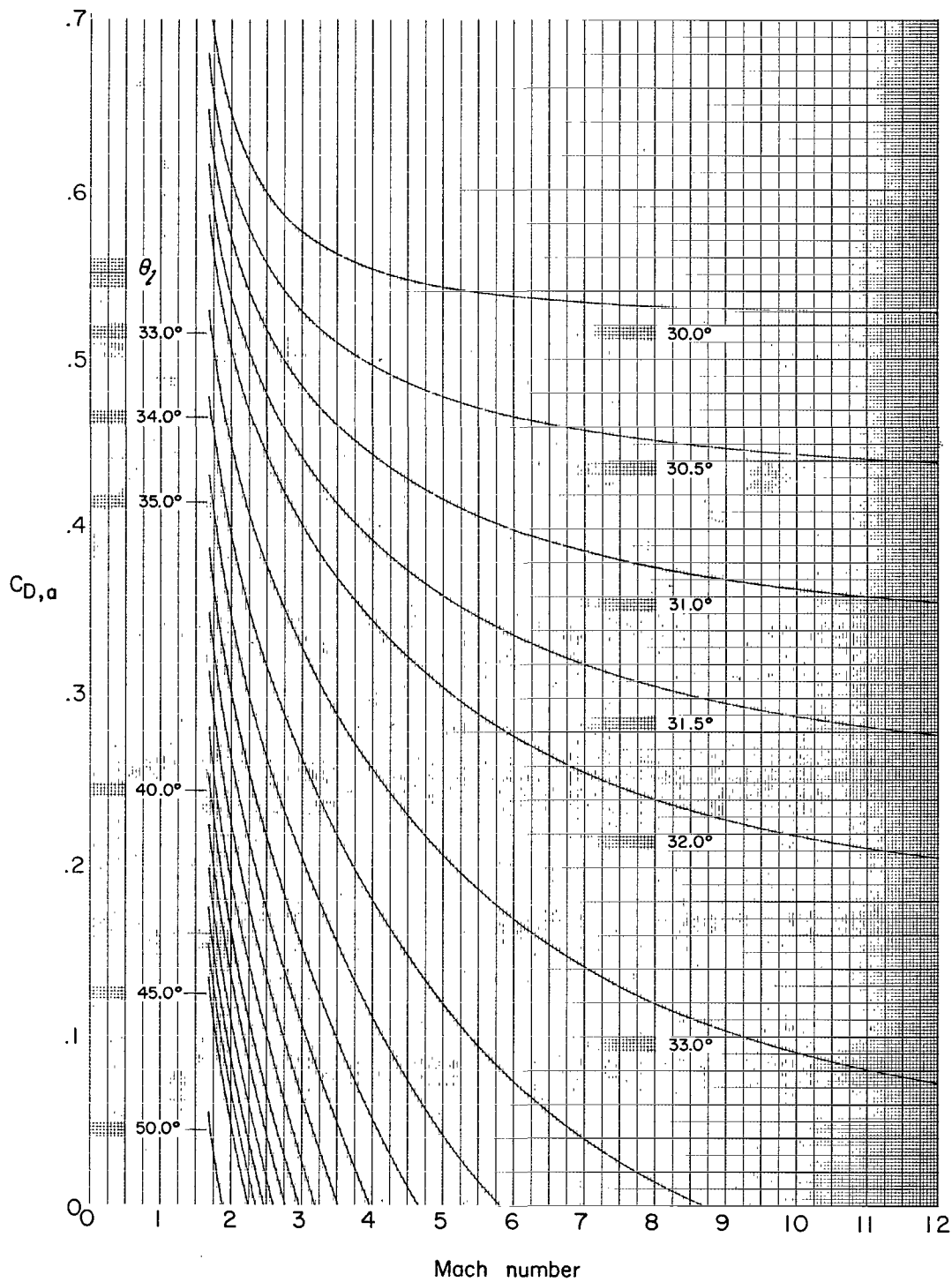
(b) Variation of mass-flow ratio with Mach number.

Figure 12.- Continued.



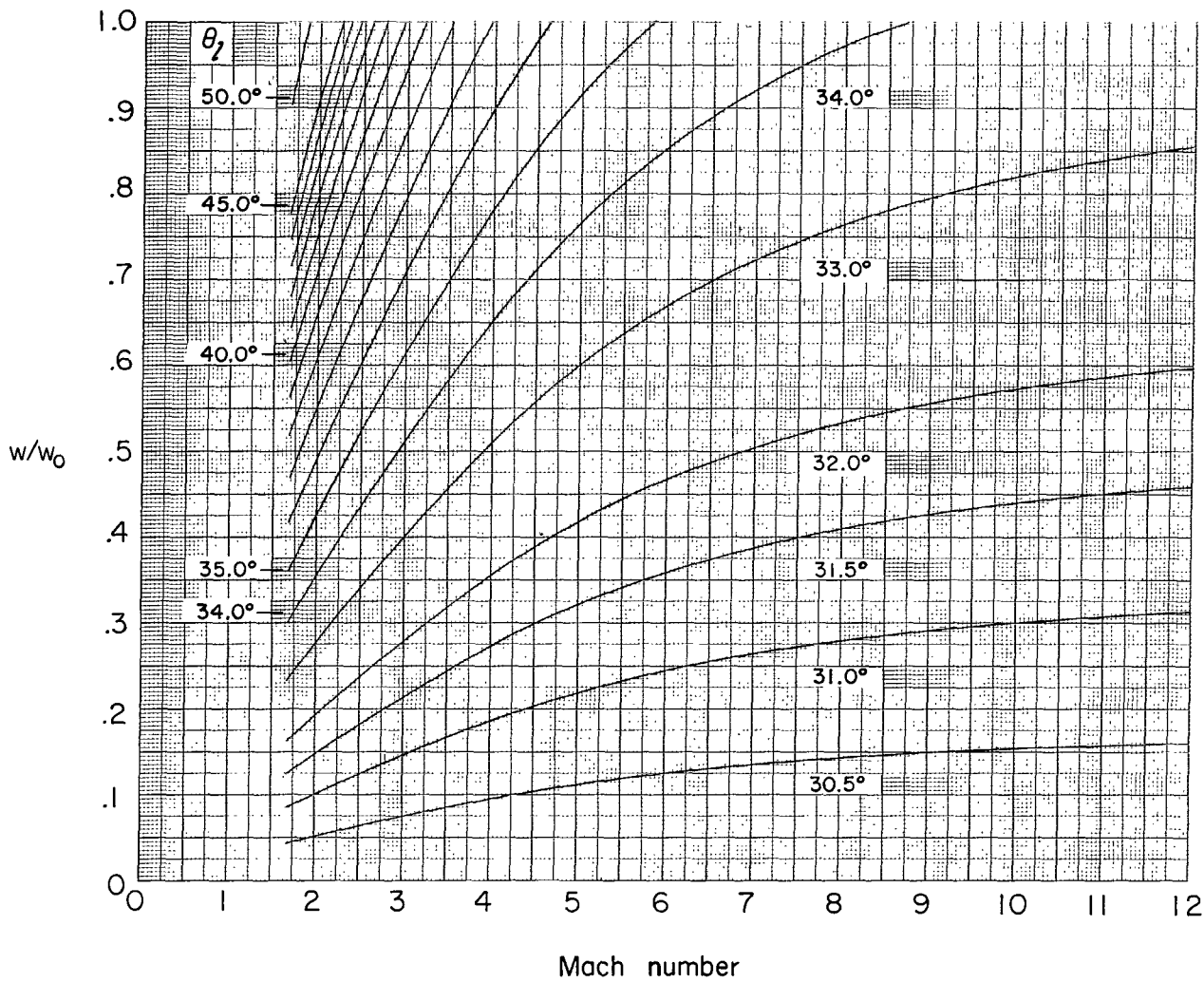
(c) Variation of additive drag with mass-flow ratio.

Figure 12.- Concluded.



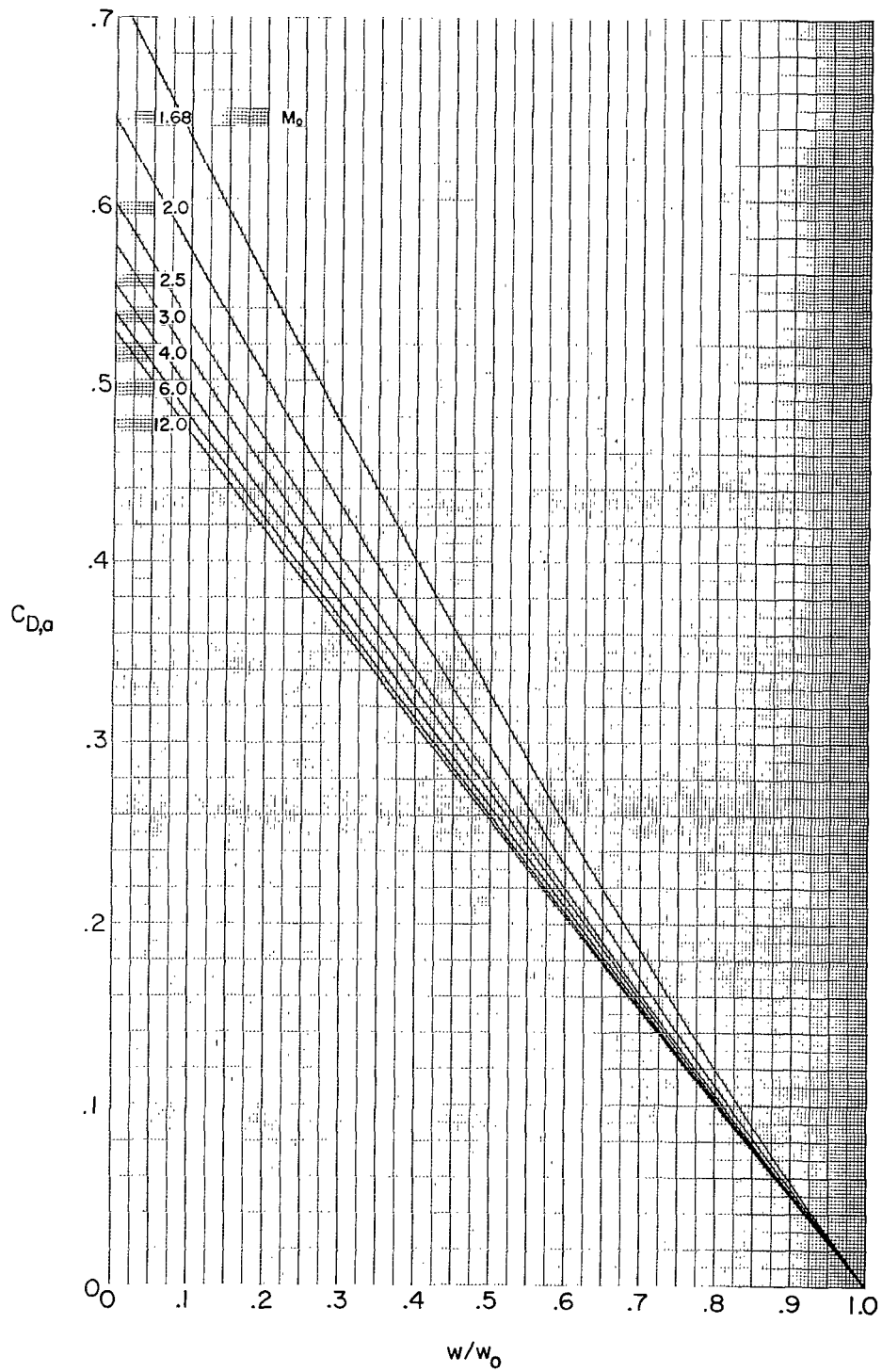
(a) Variation of additive drag with Mach number.

Figure 13.- Variation of additive drag and mass-flow ratio for  $\eta = 30^\circ$ .



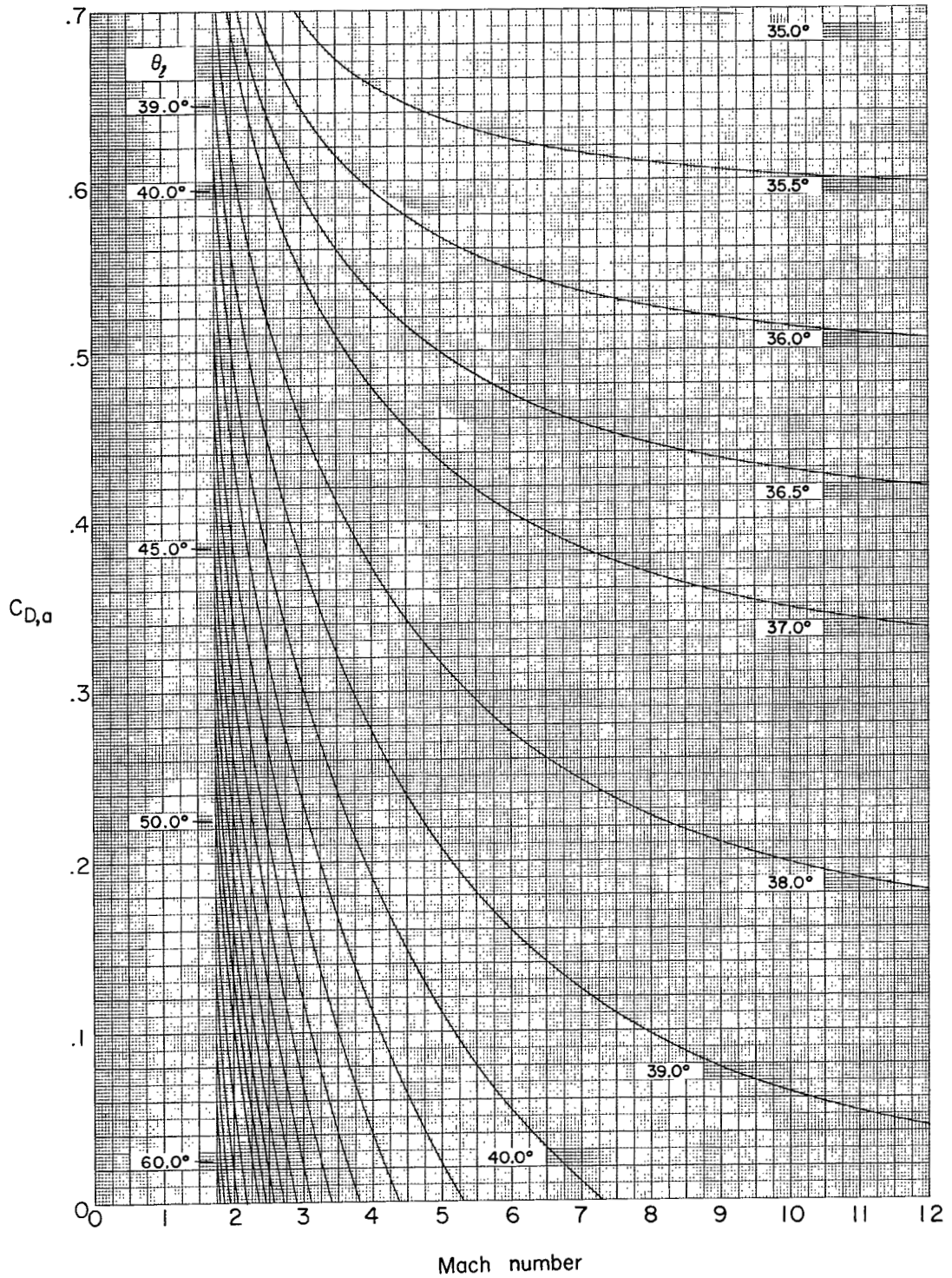
(b) Variation of mass-flow ratio with Mach number.

Figure 13.- Continued.



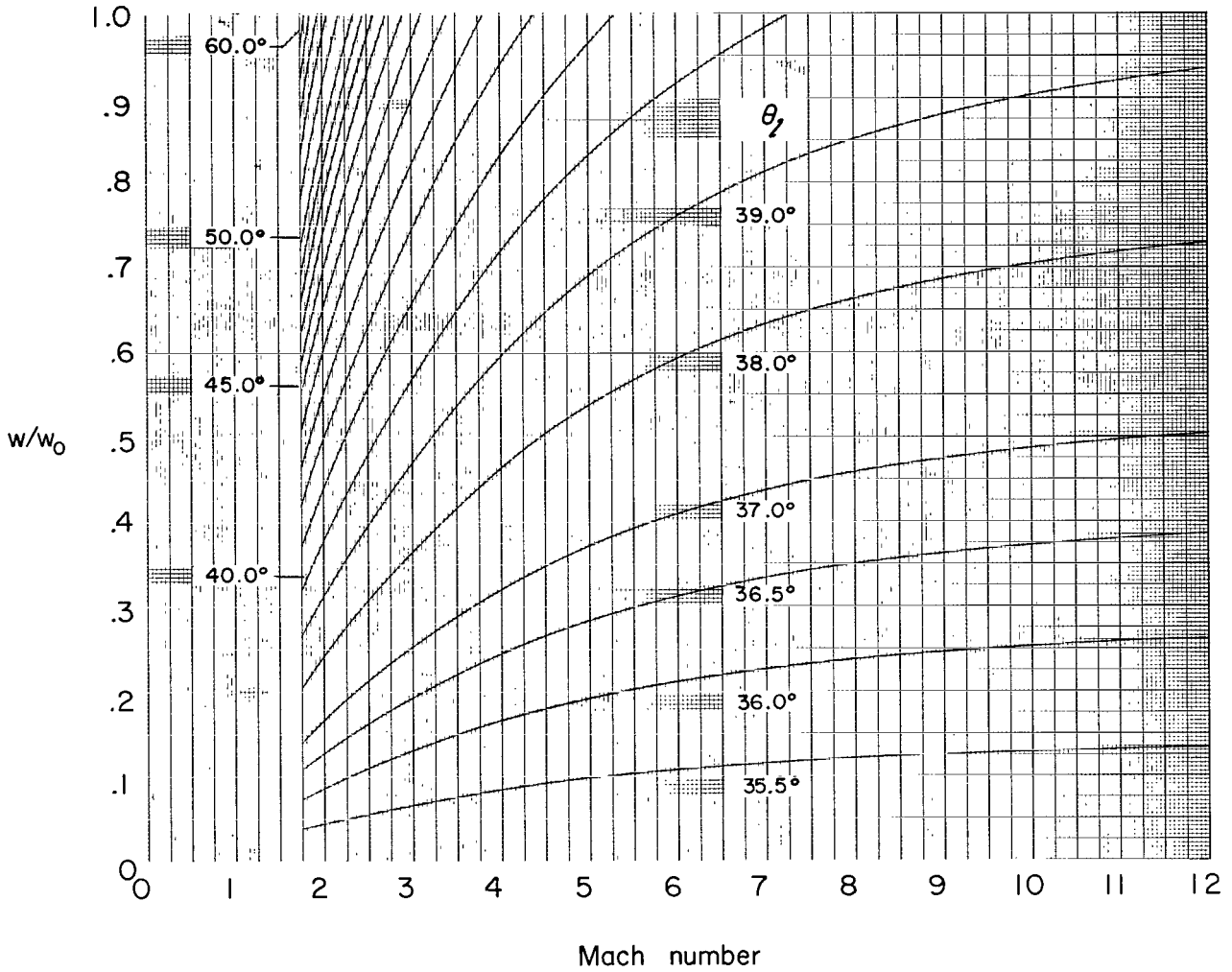
(c) Variation of additive drag with mass-flow ratio.

Figure 13.- Concluded.



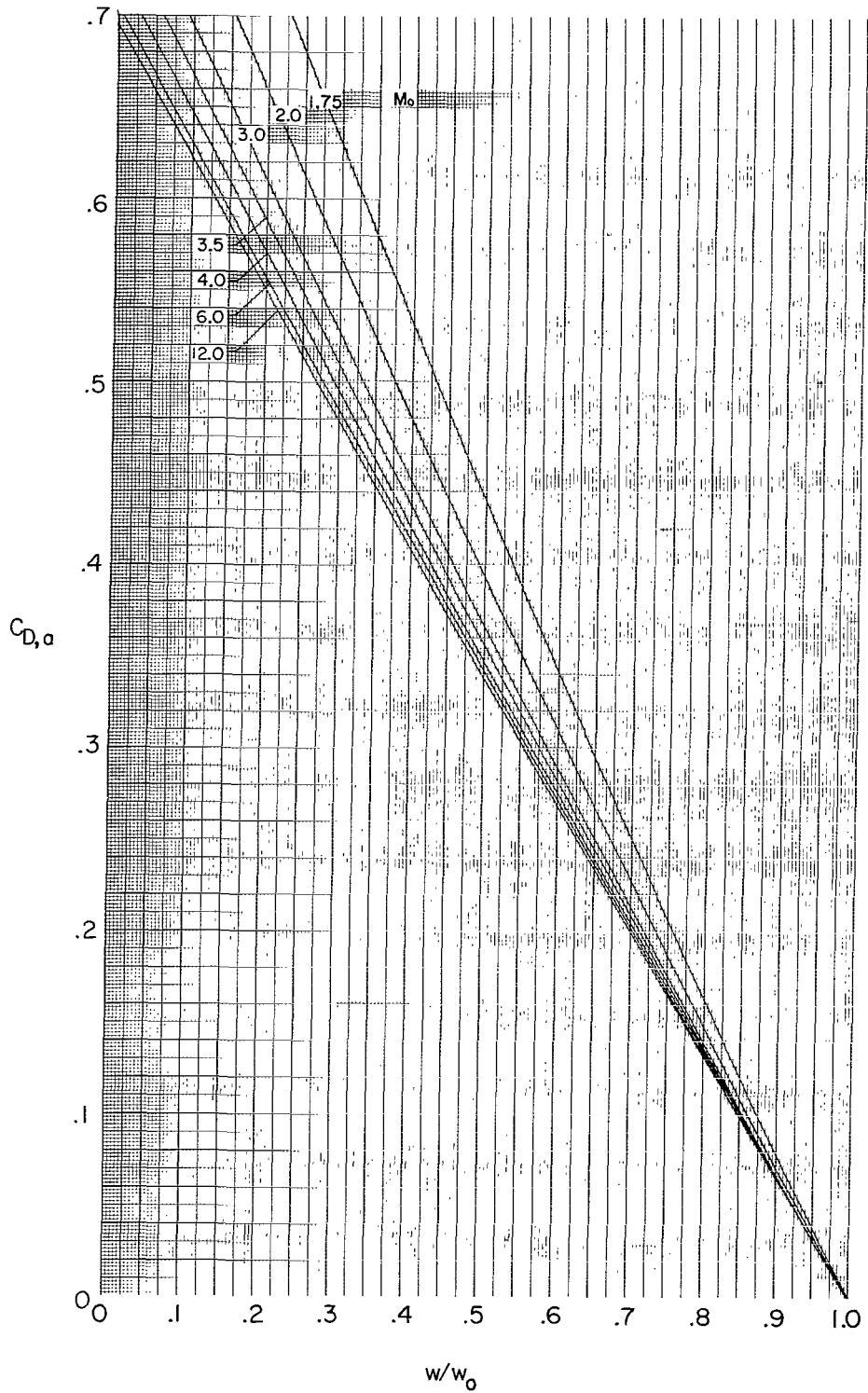
(a) Variation of additive drag with Mach number.

Figure 14.- Variation of additive drag and mass-flow ratio for  $\eta = 35^\circ$ .



(b) Variation of mass-flow ratio with Mach number.

Figure 14.- Continued.



(c) Variation of additive drag with mass-flow ratio.

Figure 14.- Concluded.

## CONCLUDING REMARKS

Working charts are presented giving values of additive drag coefficient and mass-flow ratio for inlets utilizing axisymmetric cones at zero angle of attack. Cone half-angles range from  $5^{\circ}$  to  $35^{\circ}$ . The free-stream Mach number ranges from that which will yield sonic flow on the cone surface to 12. Perfect-gas relations are used throughout the calculations.

Langley Research Center,  
National Aeronautics and Space Administration,  
Langley Station, Hampton, Va., March 2, 1966.

## REFERENCES

1. Sibulkin, Merwin: Theoretical and Experimental Investigation of Additive Drag. NACA Rept. 1187, 1954. (Supersedes NACA RM E51B13.)
2. Ames Research Staff: Equations, Tables, and Charts for Compressible Flow. NACA Rept. 1135, 1953. (Supersedes NACA TN 1428.)
3. Ferri, Antonio: Elements of Aerodynamics of Supersonic Flows. The Macmillan Co., 1949.
4. Staff of the Computing Section, Center of Analysis (Under Direction of Zdeněk Kopal): Tables of Supersonic Flow Around Cones of Large Yaw. Tech. Rept. No. 5 (NOrd Contracts No. 8555 and 9169), Massachusetts Inst. Technol., 1949. (Available from ASTIA as AD 206827.)
5. Sims, Joseph L.: Tables for Supersonic Flow Around Right Circular Cones at Zero Angle of Attack. NASA SP-3004, 1964.

*"The aeronautical and space activities of the United States shall be conducted so as to contribute . . . to the expansion of human knowledge of phenomena in the atmosphere and space. The Administration shall provide for the widest practicable and appropriate dissemination of information concerning its activities and the results thereof."*

—NATIONAL AERONAUTICS AND SPACE ACT OF 1958

## NASA SCIENTIFIC AND TECHNICAL PUBLICATIONS

**TECHNICAL REPORTS:** Scientific and technical information considered important, complete, and a lasting contribution to existing knowledge.

**TECHNICAL NOTES:** Information less broad in scope but nevertheless of importance as a contribution to existing knowledge.

**TECHNICAL MEMORANDUMS:** Information receiving limited distribution because of preliminary data, security classification, or other reasons.

**CONTRACTOR REPORTS:** Technical information generated in connection with a NASA contract or grant and released under NASA auspices.

**TECHNICAL TRANSLATIONS:** Information published in a foreign language considered to merit NASA distribution in English.

**TECHNICAL REPRINTS:** Information derived from NASA activities and initially published in the form of journal articles.

**SPECIAL PUBLICATIONS:** Information derived from or of value to NASA activities but not necessarily reporting the results of individual NASA-programmed scientific efforts. Publications include conference proceedings, monographs, data compilations, handbooks, sourcebooks, and special bibliographies.

*Details on the availability of these publications may be obtained from:*

SCIENTIFIC AND TECHNICAL INFORMATION DIVISION  
NATIONAL AERONAUTICS AND SPACE ADMINISTRATION  
Washington, D.C. 20546